이학박사학위논문

Photonic Crystal Phosphors

광자결정 형광체

2015년 8월

서울대학교 대학원

물리천문학부

민 경 택

Photonic Crystal Phosphors

by
Kyungtaek Min

Supervised by
Professor Heonsu Jeon

A Dissertation Submitted to the Faculty of
Seoul National University
in Partial Fulfillment of the Requirements
for the Degree of
Doctor of Philosophy

August 2015

Department of Physics and Astronomy
Graduate School
Seoul National University

Abstract

Photonic Crystal Phosphors

Kyungtaek Min

Majoring in Physics

Department of Physics and Astronomy

The Graduate School

Seoul National University

Photonic crystals (PCs) are photonic structures with periodically arranged index profiles. The periodicity of the PC results in a complex photonic band structure that may include a photonic band-gap (PBG), as a photonic counterpart of electronic energy band-gap under the periodic potential of a crystalline solid. Within the PBG wavelength range, light is prohibited to propagate through the PC structure. Meanwhile, photonic band-edge (PBE) modes possess many novel and unique properties. Group velocity of light with a PBE wavelength approaches zero, which makes its interaction with matter significantly stronger.

In phosphor materials, a wavelength conversion of light occurs; they absorb energy of pump photons and re-radiate photons typically at a longer wavelength. Such color-conversion phosphors have many important applications in the general lighting industry. The phosphor-capped white light-

emitting devices using light-emitting diodes (LEDs) or laser diodes (LDs) as pumping sources are recent characteristic examples of next-generation light sources for solid-state lighting. Consequently, considerable efforts have been devoted to improve the luminous efficiency of phosphors. However, most developmental works for highly efficient phosphors have focused on material aspects, such as the synthesis and adoption of new chemicals, which improve the internal quantum efficiency (IQE) of phosphor materials.

In this thesis, I suggested a new concept of PC phosphors to enhance pumping efficiency for phosphor materials. Unlike any other methods for improvement of the IQE of phosphors or the extraction efficiency of emitted light from phosphors, I paid attention to the structural aspects of phosphors and increased concentration of pump photons in the structured phosphor media. More specifically, the electric field of the PBE modes is localized in the PC phosphors, which induces strong interaction between pump photons and phosphor materials. As directions of periodicity, such as vertical and lateral, two types of the PC phosphors were demonstrated in this thesis.

Keyword: Photonic crystal, Phosphor, Photonic crystal phosphor, Photonic band-edge, Quantum dot, Laser holographic lithography

Student number: 2007-22865

Contents

List of Tables

List of Figures

Chapter 1

Introduction

1.1 Photonic Crystals

1.1.1 Introduction

Control the light propagation through artificially structured media has been studied for a long time and considered very important research topic. Above all, periodic structures have unique and interesting optical properties. Photonic crystals (PCs) refer to photonic structures with a periodically arranged index profiles [1]. PCs are defined as one-, two-, and three-dimensional PCs depending on the direction of periodicity. Figure 1-1-1 shows schematic of three types of PCs, which are realized by various fabrication methods and being applied to many useful optical devices. Scanning electron microscope (SEM) images of examples of 1D, 2D, and 3D PCs with sub-micron periods are shown in Fig. 1-1-2; Bragg reflector, band-edge laser, and opal crystal, respectively [2].

The periodicity of the PC results in a complex photonic band structure that may include a photonic band-gap (PBG), where light is prohibited to propagate through the PC structure. [1,3]. By employing PCs as a building block or backbone, photonic devices can be constructed in much smaller sizes than their conventional counterparts based on micro-photonics, and yet exhibit unprecedented performance properties and new functionalities. Many useful photonic devices operating by the PBG effects have been developed, e.g., optical cavities [4,5] and waveguides [6,7].

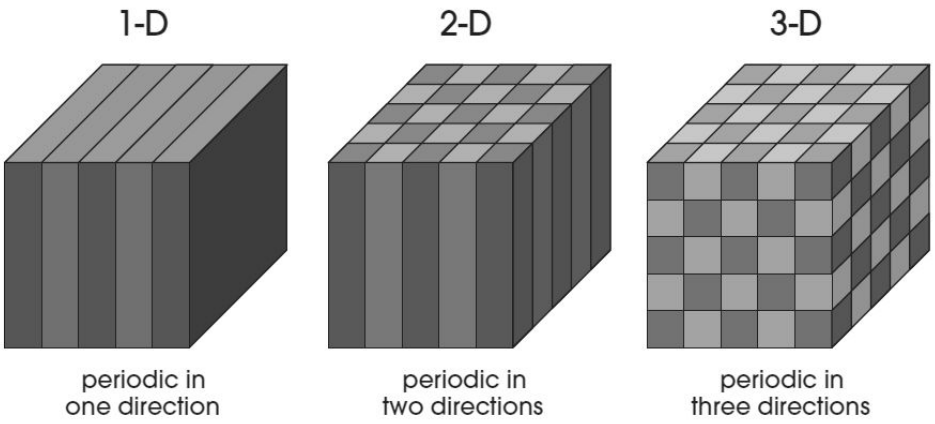

Figure 1-1-1 Schematic of representative 1D, 2D, and 3D PCs [1].

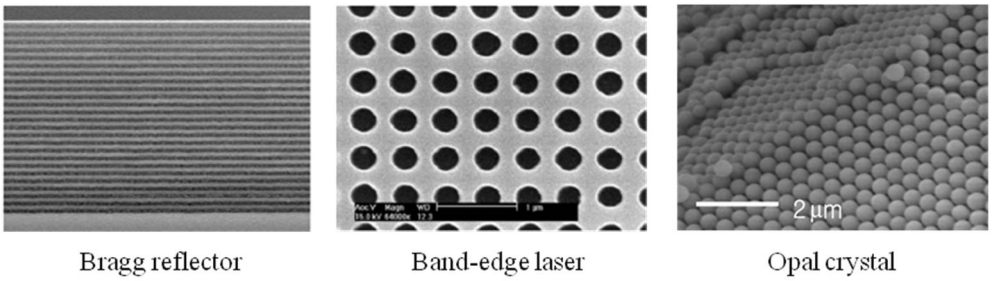

Figure 1-1-2 SEM images of examples of PCs with sub-micron periods [2].

In this thesis, I utilized a photonic band-edge (PBE) mode that possesses many novel and unique properties for PC-based phosphor structures. Among others, group velocity of light with a PBE wavelength approaches zero, which makes its interaction with matter significantly stronger [8,9]. And electromagnetic fields at PBE wavelengths form large-area resonant modes through the entire structures because PBEs are located just outside the PBGs. Finally strong light-matter interactions at large areas may occur due to the PBE effect. A PBE laser is the most representative PBE-based device, which the energy of the emitted photons is tuned to the PBE wavelength so that the optical gain is enhanced, and thus lasing action occurs [10,11]. In another example, a PBE mode was used to set the conditions for the improvement of the absorption efficiency of solar cells [12-14]. It is the latter case that the present work shares the basic principle. Meanwhile, I suggested *efficient optical pumping method* based on the PBE effect.

1.1.2 Photonic crystals and electronic crystals

We can draw an analogy between photonics and electronics. The PBG is a photonic counterpart of electronic energy band-gap under the periodic potential of a crystalline solid. Table 1-1-1 shows fundamental similarities between photonics and electronics. In electronics, scalar wave function $\Psi(\mathbf{r})$ of distribution probability of one electron can be found by solving Schrödinger equation with the periodic potential $V(\mathbf{r})$. Figure 1-1-3(a) shows dispersion relation between momentum and energy of one electron. Unlike the case of a free electron, periodicity of potential of a solid crystal causes energy band-gap where the electron cannot exist. Similarly in photonics, the propagation of light is described using magnetic field vector $\mathbf{H}(\mathbf{r})$. With periodic permittivity $\varepsilon(\mathbf{r})$, solutions of Maxwell's equations provide dispersion relation between frequency of electromagnetic wave and wave vector $\mathbf{k}$. Forbidden photonic band-gap in which light cannot propagate exists particular frequency ranges, shown in Fig. 1-1-3(b).

This resemblance of behaviors between photons and electrons is contributing to understanding fundamentals of PCs and adoption of unique properties in advanced electronics for photonic counterpart devices or photonic circuits.

Electronic Crystal	Photonic Crystal
Periodic electronic potential	Periodic dielectric distribution
Electronic band-gap	Photonic band-gap
Schrodinger equation $\left[-\frac{\hbar^2}{2m}\nabla^2 + V(\mathbf{r})\right]\psi_E(\mathbf{r}) = E\,\psi_E(\mathbf{r})$	Maxwell equation $\nabla \times \frac{1}{\varepsilon(\mathbf{r})}\nabla \times \mathbf{H}_\omega(\mathbf{r}) = \frac{\omega^2}{c^2}\mathbf{H}_\omega(\mathbf{r})$

Table 1-1-1 Comparison between electronic crystals and photonic crystals.

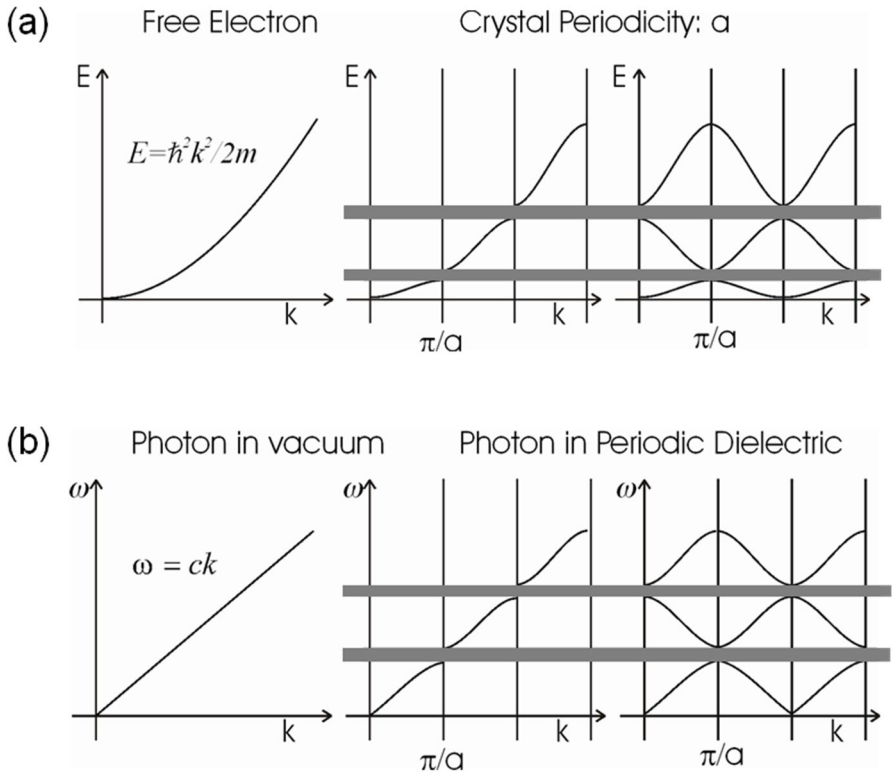

Figure 1-1-3 Dispersion relation between (a) momentum and energy of one electron in an electronic crystal, (b) frequency of electromagnetic wave and wave vector **k** in a photonic crystal [1].

1.2 Phosphors

1.2.1 Luminous efficiency of phosphors

In phosphor materials, a wavelength conversion of light occurs; they absorb energy of pump photons and re-radiate photons typically at a longer wavelength. Such color-conversion phosphors have many important applications in the general lighting industry. Figure 1-2-1 shows the phosphor-adopted light-emitting devices using light-emitting diodes (LEDs) or laser diodes (LDs) as pumping sources, which are recent characteristic examples of next-generation light sources for solid-state lighting [15, 16].

A conversion efficiency of phosphors as wavelength converters from pump photons with higher energy to emitted photons with lower energy, or the external quantum efficiency (EQE) η_{external} is given by

$$\eta_{\mathrm{external}} = (\text{Absorbance of pump photons by phosphors}) \times \eta_{\mathrm{internal}} .$$

The ratio of number of photons emitted from the phosphor molecules to number of pump photons absorbed by phosphors is defined as the internal quantum efficiency (IQE) η_{internal}, which depends on inherent characteristics of phosphor materials.

Considerable efforts have been devoted to improve the luminous efficiency of phosphors. However, most developmental works for highly efficient phosphors have focused on material aspects, such as the synthesis and adoption of new chemicals, to improve the IQE of phosphor materials.

In popular dichromatic white LEDs, yellow YAG phosphors are pumped by blue light emitted from gallium nitride light-emitting LEDs and combined emission

spectrum of the phosphor-based white LEDs consists the blue luminescence band and the yellow phosphorescence band, as shown in Fig. 1-2-2. Generally emission intensity from phosphors and the shape of entire emission band from white LEDs are determined by the thickness of phosphor layer and the concentration of phosphor materials.

Meanwhile, I suggested fresh methods to improve pump efficiency of phosphor without adopting new kinds of chemicals or increasing phosphor molecules spatially. I just distributed existing phosphor materials in the form of PCs and controlled the pump light propagation to strengthen interaction between pump photons and phosphor materials to increase absorbance of pump photons by the phosphor materials, which were caused by the PBE effect.

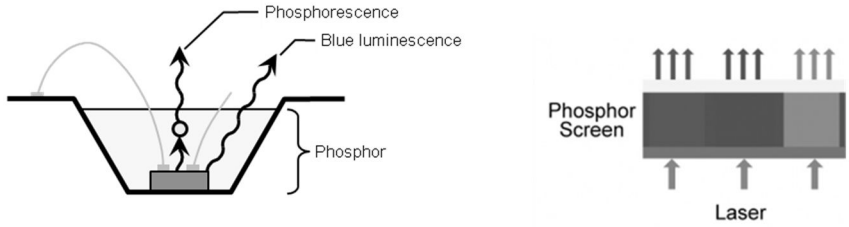

White LED (Light-emitting diode)　　Laser phosphor display (LPD)

Figure 1-2-1 Phosphor-adopted light-emitting devices using light-emitting diodes (left) [15] or laser diodes (right) [16] as pumping sources.

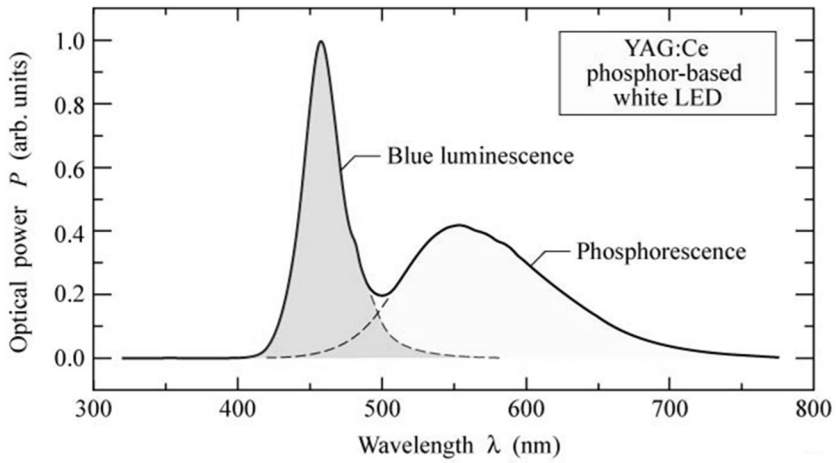

Figure 1-2-2 Emission spectrum of a phosphor-capped white LED [15].

1.2.2 Photonic crystal phosphors

In this thesis, I suggested a new concept of PC phosphors to enhance pumping efficiency for phosphor materials. Unlike any other methods for improvement of the IQE of phosphors or the extraction efficiency of emitted light from phosphors, I paid attention to the structural aspects of phosphors and increased concentration of pump photons in the structured phosphor media. More specifically, the electric field of the PBE modes is localized in the PC phosphors, which induces strong interaction between pump photons and phosphor materials. As directions of periodicity, such as vertical and lateral, two types of the PC phosphors were characterized in this thesis, which is shown in Fig. 1-2-3.

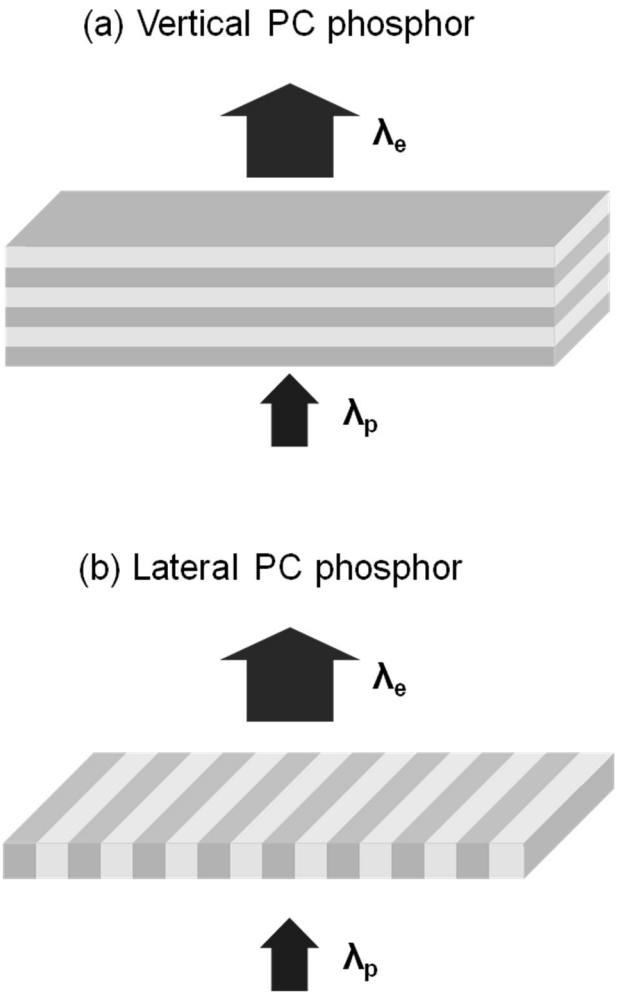

Figure 1-2-3 Two types of PC phosphors characterized by directions of periodicity. (a) Vertical PC phosphor and (b) lateral PC phosphor.

1.3 Computational Method

1.3.1 Plane-wave expansion method

Plane-wave expansion (PWE) method, which is a method to get solutions of Maxwell's equations in infinitely periodic media, is very powerful technique and suitable to investigate the photonic band structure of any types of PCs. To solve Maxwell's equations, electric fields and magnetic fields are expanded in terms of Fourier components along their reciprocal lattice vector. These differential equations are formulated to an infinite-size matrix eigenvalue problem, which can be solved after proper approximation [17,18]

I used commercially available computer software, BandSOLVE (Rsoft Design Group), which simulation methods are based on the PWE, to investigate the photonic band structure of the one-dimensional (1D) vertical PCs in chapter 2.

1.3.2 Transfer-matrix method

Within the framework of the ray optics, transfer-matrix (TM) method is an effective method to describe light propagation through various media. From the Maxwell's equations we can get two matrices about behavior of photons propagating in homogeneous media and exceeding the boundary between separate media, respectively. Based on the two kinds of matrices, wave equations of electromagnetic waves passing through various media can be solved finally, which process is somewhat simple as one can solve analytically by hand. [19]

Furthermore, wave equations can be solved exactly by adopting analytic solutions to computer software products like MATLAB, Mathematica, Mathcad, and so on. The Mathcad was used to investigate reflectance, transmittance, and absorbance of the vertical PC phosphors in chapter 2 by the TM method.

1.3.3 Finite-difference time-domain method

Finite-difference time-domain (FDTD) method is a widely used numerical method in which space is divided into a discrete grid like a mesh then each of the electric fields and magnetic fields are developed in discrete time steps. Unlike former methods with approximations in processes or limitations in boundary conditions, most solutions of the time dependent Maxwell's equations can be solved exactly and the accuracy depends on the size of the grids and time steps [20].

Due to advantages of the FDTD method, various computer software products are developed commercially and I used Lumerical FDTD Solutions (Lumerical Solutions, Inc.) to explore the photonic band structures, electric field profiles of the PBE modes, and absorbance of the lateral PC phosphors in chapter 3.

1.4 Outline of the Manuscript

As mentioned above, I suggested a new concept of PC phosphors to enhance pumping efficiency for phosphor materials. Two types of PC phosphor structures are modeled and fabricated for that purpose and I measured photoluminescence (PL) intensity from the PC phosphors with a wavelength-tunable pump system.

In chapter 2, the vertical PC phosphors were suggested. I investigated optical properties of the vertical PC structures and modeled suitable PC phosphors to observe PBE effect by computational method such as TM and PWE. The vertical PC phosphors were fabricated by spin-coating method and PBE effect and PL enhancements were confirmed experimentally.

In chapter 3, I proposed the lateral PC phosphors which fabrication steps are refined and performance of PL enhancement are improved. FDTD simulation tool was used to simulate PBE modes of the lateral PCs. I focused on shortcomings of previous vertical PC phosphors and raised applicability of real light-emitting devices. The lateral PCs were patterned by laser holographic lithography (LHL) and PL from the lateral PC phosphors was investigated with similar PL measurement setup in chapter 2. PL enhancement at the Γ-point PBE wavelength and polarization dependence of the pump source on the PBE effect were verified.

Finally in chapter 4, the conclusion is presented.

References

[1] John D. Joannopoulos, Robert D. Meade, and Joshua N. Winn, *Photonic crystals: Molding the flow of light* (Princeton University Press 2008).

[2] http://mnoel.snu.ac.kr/

[3] E. Yablonovitch, "Inhibited spontaneous emission in solid-state physics and electronics," Phys. Rev. Lett. **58**, 2059-2062 (1987).

[4] H. Yokoyama, "Physics and device applications of optical microcavities," Science **256**, 66-70 (1992).

[5] O. Painter, R. K. Lee, A. Scherer, A. Yariv, J. D. O'Brien, P. D. Dapkus, and I. Kim, "Two-dimensional photonic band-gap defect mode laser," Science **284**, 1819-1821 (1999).

[6] C. J. M. Smith, H. Benisty, S. Olivier, M. Rattier, C. Weisbuch, T. F. Krauss, R. M. De La Rue, R. Houdré, and U. Oesterle, "Low-loss channel waveguides with two-dimensional photonic crystal boundaries," Appl. Phys. Lett. **77**, 2813-2815 (2000).

[7] Y.-G. Roh, S. Yoon, H. Jeon, S.-H. Han, and Q-H. Park, "Experimental verification of cross talk reduction in photonic crystal waveguide crossings," Appl. Phys. Lett. **85**, 3351-3353 (2004).

[8] T. Baba, "Slow light in photonic crystals," Nat. Photonics **2**, 465 (2008).

[9] S. John, and T. Quang, "Spontaneous emission near the edge of a photonic band gap," Phys. Rev. A **50**, 1764 (1994).

[10] J. P. Dowling, M. Scalora, M. J. Bloemer, and C. M. Bowden, "The photonic band edge laser: A new approach to gain enhancement," J. Appl. Phys. **75**, 1896

(1994).

[11] S. Kim, S. Ahn, K. Min, S. Kim, H. Jeon, P. Regreny, and C. Seassal, "Nano Stepping-Stone Laser," Appl. Phys. Express **6**, 042703 (2013).

[12] D. Y. Zhou and R. Biswas, "Photonic crystal enhanced light-trapping in thin film solar cells," J. Appl. Phys. **103**, 093102 (2008).

[13] C. M. Johnson, P. J. Reece, and G. J. Conibeer, "Slow-light-enhanced upconversion for photovoltaic applications in one-dimensional photonic crystals," Opt. Lett. **36**, 3990 (2011).

[14] Y. Park, E. Drouard, O. El Daif, X. Letartre, P. Viktorovitch, A. Fave, A. Kaminski, M. Lemiti, and C. Seassal, "Absorption enhancement using photonic crystals for silicon thin film solar cells," Opt. Express **17**, 14312 (2009).

[15] E. F. Schubert, *Light-Emitting Diodes* (Cambridge University Press 2006).

[16] http://www.xconomy.com/

[17] K.-M. Ho, C. T. Chan, and C. M. Soukoulis, "Existence of a photonic hap in periodic dielectric structures," Phys. Rev. Lett. **65**, 3152 (1990).

[18] R. D. Meade, A. M. Rappe, K. D. Brommer, J. D. Joannopoulos, and O. L. Alerhand, "Accurate theoretical analysis of photonic band-gap materials," Phys. Rev. B. **48**, 8434 (1993).

[19] P. Yeh, *Optical Waves in Layered Media* (Wiley 1988).

[20] K. S. Yee, "Numerical solution of initial boundary value problems involving Maxwell's equations in isotropic media," IEEE Trans. Antennas Propag. **14**, 302 (1996)

Chapter 2

Vertical Photonic Crystal Phosphor

2.1 Introduction

The vertical PCs refer to PCs which direction of the periodicity is perpendicular to the surface. The 1D PC introduced here is a standard distributed Bragg reflector (DBR), which consists of layers of two materials with different refractive indices stacked alternately. Because normal incident light which wavelength is included in the PBG region is reflected perfectly by the DBR, DBRs usually play a role as a optical building block in many useful optical devices, e.g., mirrors, optical cavities, and vertical-cavity surface-emitting lasers (VCSELs).

There are various fabrication methods to construct DBRs, however, active light-emitting agents must be included inside the DBRs to fabricate the vertical PC phosphors and make DBRs optically active structures themselves.

The porous silicon Bragg reflector is one example of the optically active structures. By electro-chemical etching (ECE) process, DBRs with very delicate sub-micron scale can be constructed and also, porous silicon can emit photons by optical pumping. However, absorbance of porous silicon itself in visible range of light is too strong to cause sufficient optical gain, and that is a material reason why porous silicon is unsuitable for the PC phosphor.

Electron beam or thermal evaporation of luminescent materials is a popular example of optically active thin-film fabrication. Unfortunately, deposition rates of

the evaporation of active materials is usually very low to make thin films with high quality and there are too much waste of time and costs.

In this chapter, I modeled the vertical PC phosphors [1] and also fabricated polymer-based vertical PCs by the spin-coating method [2]. CdSe/ZnS core-shell quantum dots (QDs) were embedded in a polymer material as phosphor. Materials including QDs, polymers, and solutions are commercially available and I could adjust the thickness of thin films and the PBG wavelength of the vertical PC very exactly and comfortably by controlling concentration of solutes and rotational speeds in spin coating steps.

While combined devices of DBRs and active materials ever developed are using the PBG effect as principle of operation, the PC phosphors are based on the PBE effect and I will prove an idea of the PC phosphor in this chapter.

2.2 Model Calculation

General optical properties of the vertical PCs, such as reflectance and transmittance, are need to be investigated and then PBG wavelengths may be distinguished from the reflectance and transmittance spectra. I checked over the photonic band structures of the vertical PCs by the PWE method and also calculated reflectance, transmittance and electric field profiles within the vertical PC structures by the TM method.

In case of the vertical PC phosphors, in which active light-emitting materials embedded, absorbance by the phosphor materials exists and result in PL from the phosphors. In this thesis, I assumed the IQE of phosphor materials is unity and the PL from the phosphors is then simply proportional to the absorbance of pump photons. This assumption should be reasonable as long as active light-emitting agents are scarce enough within the PC phosphor structure so that absorption does not affect much features of the photonic band structure of the vertical PCs. The influence of phosphor concentrations will be discussed in the latter of this chapter.

The object of chapter 2.2 is to facilitate the understanding of optical properties of vertical PCs and fundamentals of the PBE effect of the vertical PC phosphors. For that purpose, I assumed structure materials of the vertical PC phosphors which have a large difference in refractive indices. The vertical PC model structure considered in chapter 2.2 consists of layers of two materials which refractive indices are n_L = 1.45 (for low index materials) and n_H = 1.76 (for high index materials), which are the typical refractive indices of silica and alumina, respectively. Figure 2-2-1 is a schematic of the vertical PC phosphor. And the thickness of each layer is given by $d_i = \lambda_0/4n_i$ (i = L, H), where λ_0, the center wavelength of the PBG, is

chosen to be 420 nm. Light-emitting phosphor materials are assumed to be dispersed only in the layers in the structure that have a high refractive index. The rationale for this assumption is explained in chapter 2.2.2. The total number of pairs of alternating layers is N.

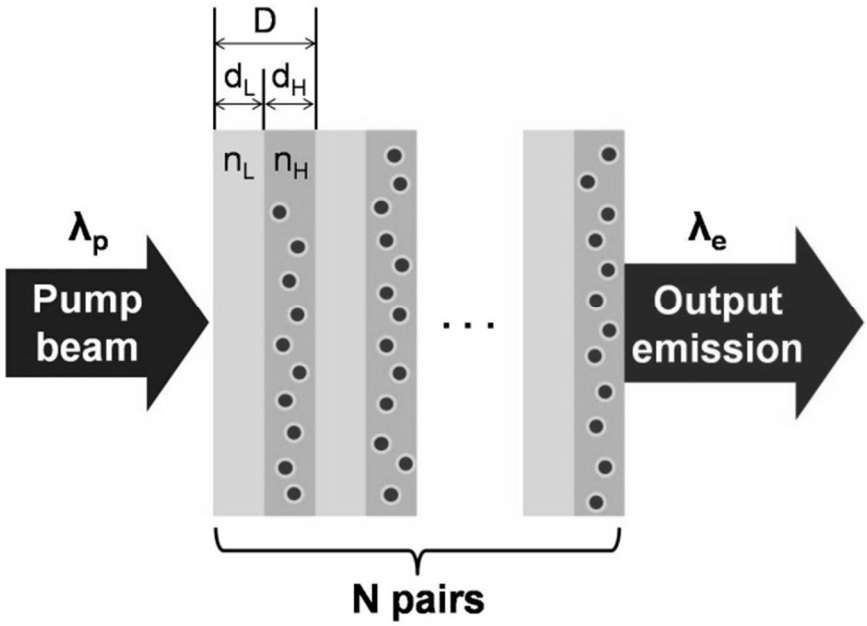

Figure 2-2-1 A schematic of the vertical PC phosphor structure consisting of N pairs of alternating layers. The refractive indices are n_L = 1.45 and n_H = 1.76. The thickness of each individual layer is $d = \lambda_0/4n$, where λ_0 is the center wavelength of PBG. The circular dots represent fluorescent agents, which are assumed to be selectively dispersed in the layers with high refractive index only.

2.2.1 Optical properties of vertical photonic crystals

The PWE method allows the exact photonic band structures of an infinite-sized PC to be determined. I calculated the photonic bands of the model vertical PC and shown in Fig. 2-2-2(a) is a diagram of the photonic band structures using this method. A PBG and PBEs on both sides of the PBG can be clearly identified in the band structure of the vertical PC. I called the first photonic band in the lower frequency region the *high index band* (HIB) and the second band in the higher frequency region the *low index band* (LIB), which correspond to the "dielectric" and "air" bands in reference [3].

In contrast to the PWE method, the TM method is suitable for investigating the optical properties, such as the reflectance, transmittance, and absorbance, of finite-sized 1D PCs [4]. Figure 2-2-2(b) displays the reflectance (R) and transmittance (T) spectra of our model vertical PC structures for N = 10 and 30 pairs of layers in the PC, which were calculated using the TM method. As the number of pairs of layers increases, the reflectance and transmittance approach 1 and 0, respectively, within the stop-band of the DBR structure (or the PBG of the vertical PC), which makes the PBEs on both sides of the PBG more discernible. The resultant PBG matches with that calculated by the PWE method and shown in Fig. 2-2-2(a). The TM method also provides the electromagnetic field profile across the entire vertical PC and enables us to anticipate various photonic properties of the PC structure, which will be will be discussed in the next session.

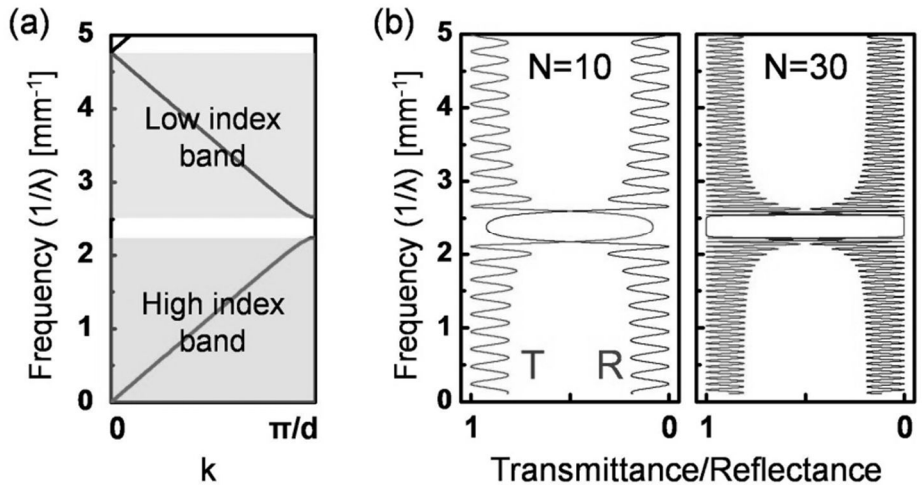

Figure 2-2-2 Photonic properties of the 1D PC. (a) Photonic band structure calculated by the PWE method. (b) Reflectance (marked with "R") and transmittance (marked with "T") spectra for N = 10 and 30.

2.2.2 Electric field profiles in vertical photonic crystal phosphors

I examined electromagnetic field profiles within the vertical PC structure at various pump photon wavelengths, utilizing the TM method. As shown in Fig. 2-2-3, the peaks in the electric field amplitude tend to correspond to the position of PC layers with a high refractive index if the pump wavelength is tuned to be within the HIB. In contrast, when the pump wavelength is tuned to be within the LIB the electric field amplitude coincides better with the positions of the PC layers with the low refractive index. This is the reason for the names “HIB” and “LIB”. Consequently, if a vertical PC structure is to be adopted for phosphor applications, it is only necessary to embed phosphor materials in the either high or low refractive index layers when the pump photon wavelength belongs to the HIB or LIB, respectively.

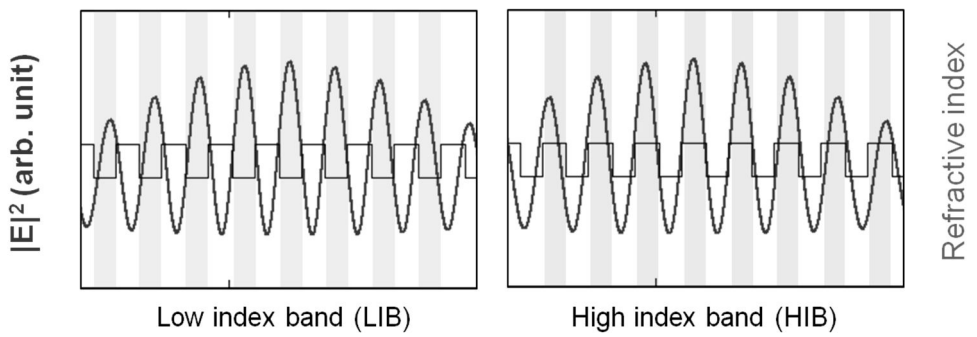

Figure 2-2-3 Electric field intensity profiles within the vertical 1D PC structure at PBE wavelengths in LIB (left) and HIB (right).

Note that a large overlap between the electric field and dipole oscillators results in a high optical transition probability and, therefore, strong photon emission [5]. If the pump photon wavelength is within the LIB, the wavelength of emitted photons, which is typically longer than the pump photon wavelength, may fall in the PBG of the PC structure. This may result in poor photon escape even if enhanced phosphor excitation occurs. For this reason, I considered the case where the pump wavelength lies within either the PBG or the HIB, and not the LIB.

Figure 2-2-4(a) shows the reflectance spectrum of our model vertical PC structure containing $N = 30$ pairs of layers. λ_1 and λ_3 are the wavelengths of the first and the second reflectance minima in the HIB region, while λ_2 is the wavelength of the first reflectance maximum between λ_1 and λ_3. For the particular 1D PC structure considered here, the representative pump wavelengths are $\lambda_0 = 420$ nm, $\lambda_1 = 451.6$ nm, $\lambda_2 = 455.5$ nm, and $\lambda_3 = 461.9$ nm.

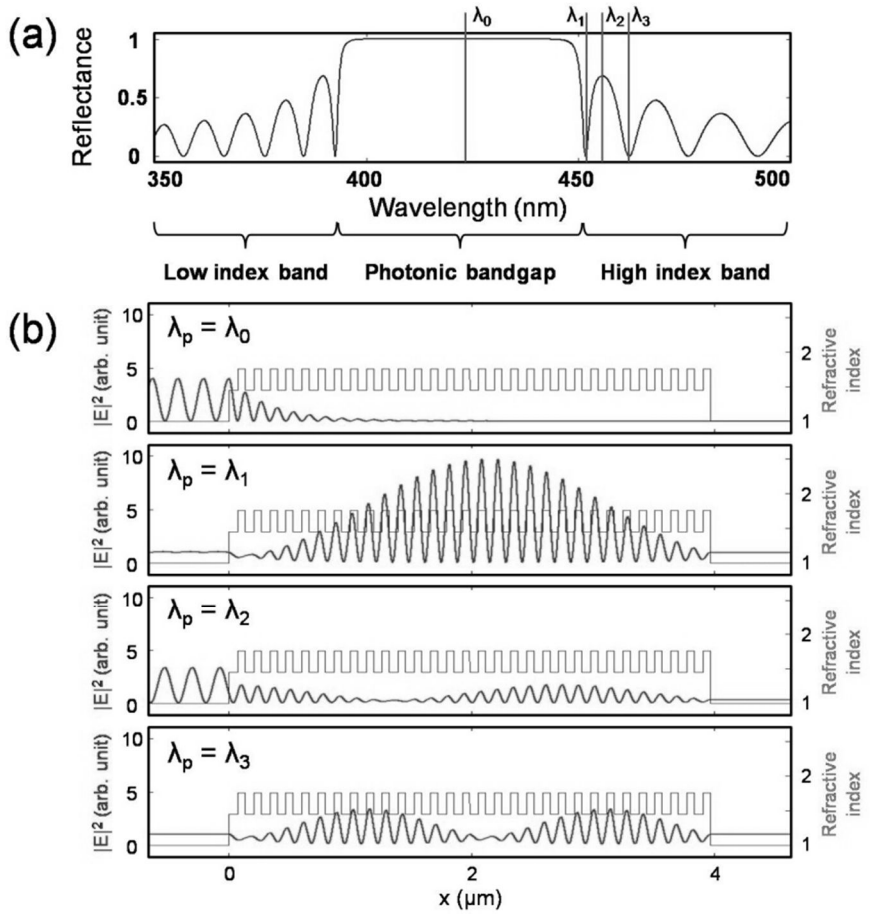

Figure 2-2-4 (a) Reflectance spectrum of the $N = 30$ vertical 1D PC structure. λ_0, λ_1, λ_2, and λ_3 indicate some of the critical and representative wavelengths in the reflectance spectrum. (b) Electric field intensity profiles when the light of each representative wavelength (λ_0, λ_1, λ_2, and λ_3) is incident from the left.

Shown in Fig. 2-2-4(b) are the electric field intensity profiles inside the vertical PC structure when light is incident from the left at the specific wavelengths of λ_0, λ_1, λ_2, and λ_3. It can be seen from Fig. 2-2-4(b) that the incident photons that have the same wavelength as the PBG center (i.e., $\lambda_p = \lambda_0$) are completely reflected by the PC structure, while the electric field intensity inside the structure rapidly decays along the propagation axis. Incident photons with a wavelength matching the wavelength of the first reflectance maximum ($\lambda_p = \lambda_2$) show a similar tendency, although an extra lobe of low intensity appears within the PC after the initial decay. In contrast, the incident photons with wavelengths of the zero of reflectance (i.e., $\lambda_p = \lambda_1$ or λ_3) exhibit features similar to *resonant tunneling*; this is often identified by the formation of a standing wave with large field amplitudes across the PC structure. The intensity envelope for λ_1 is single-lobed while that for λ_3 is double-lobed. It is also worth noting that, for $\lambda_p = \lambda_1$ or λ_3, the electric field intensity maxima coincide with the high refractive index layers, as those two wavelengths belong to the HIB. As a consequence, photons of wavelength λ_1 or λ_3 are expected to interact strongly with the high refractive index material in the 1D PC, if any optically active agent exists there. This may lead to a novel phosphor structure, which may have the potential for efficient pump photon absorption and thus strong fluorescence. In fact, there have been reports on enhanced optical phenomena due to slow light at PBEs [6-8].

2.2.3 Absorption enhancement factor

We now turn our attention to the performance characteristics of the vertical PC structure as a phosphor. Because a phosphor absorbs pump photons, its refractive index should be expressed by a complex number, e.g., $n - i\kappa$. Hence, reflectance and transmittance should be recalculated using this complex refractive index. It should be noted that in the present case only the refractive index of the high refractive index layer needs to be expressed as a complex number because we assume that phosphor materials are dispersed only in the layers of high refractive index. Absorbance (A) is then deduced from reflectance and transmittance using the simple energy conservation law, i.e., $A = 1 - R - T$. In order to estimate the PL intensity, we assume that the internal quantum efficiency of the phosphor is unity. The PL intensity from the phosphor materials is then simply proportional to the absorbance of the pump photons. This assumption should be reasonable as long as phosphor materials are scarce enough within the structure (so that absorption does not alter much the band structure properties of the vertical PC) and at the same time the pump intensity is kept low (so that phosphor molecules remain unsaturated). I chose CdSe/ZnS core-shell QDs as the phosphor in the model calculations, which have been drawing attention as a new nano-photonic material with a strong light-emitting ability [9]. The molar absorption coefficient (or molar absorptivity) of the QDs is taken from previous studies to be $\varepsilon = 10^5$ $cm^{-1}M^{-1}$ [10], while the QD molar concentration is assumed to be 10^{-4} M.

In the following text, I compare the vertical PC phosphor with a bulk phosphor, which is formed by removing all the layers with a low refractive index from the corresponding vertical PC phosphor, thus ensuring that the reference bulk phosphor contains the same amount of QDs as the vertical PC phosphor. The difference

between the two samples is that one has a periodicity in the refractive index profile, while the other does not. Therefore, we may attribute any change in PL to this structural difference. Finally, the overall enhancement factor in PL can be expressed by the absorbance ratio between the PC phosphor and its bulk counterpart as we have already assumed that PL intensity is proportional to the absorbance of pump photons; it is therefore implicit that the PL enhancement factor corresponds to the enhanced luminescence in the total solid angle of 4π steradians.

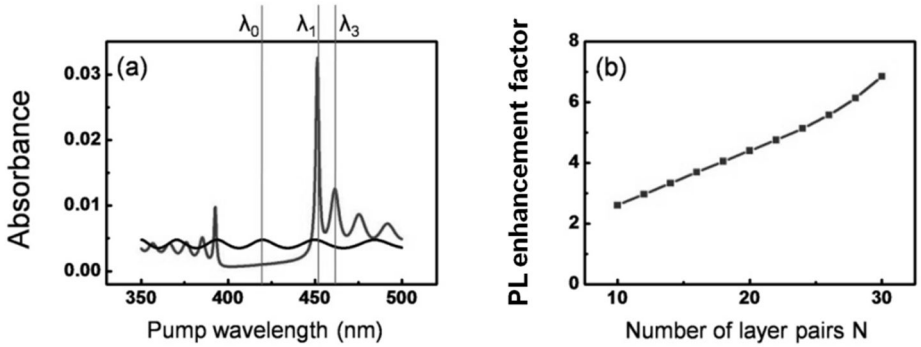

Figure 2-2-5 Phosphor characteristics of the vertical PC phosphor and bulk phosphor when pumped by a monochromatic light source. (a) Absorbance spectra of the vertical PC phosphor with N = 30 pairs of layers (gray line) and of the bulk phosphor with equivalent phosphor thickness (black line), as a function of monochromatic pump wavelength. (b) PL enhancement factor of the vertical PC phosphor as a function of the number of pairs of layers.

Figure 2-2-5(a) compares the absorbance of the vertical PC phosphor with that of the bulk phosphor as a function of the pump photon wavelength, λ_p. At $\lambda_p = \lambda_0 =$ 420 nm (the center of the PBG), pump photons are subject to total reflection except for those penetrating a finite distance into the phosphor, because propagation of photons through the PC phosphor is strictly forbidden. This results in poor excitation of phosphors, *i.e.*, QDs. Thus the condition $\lambda_p = \lambda_0$ (more generally, pumping the PC phosphor at any wavelength within the PBG) is unsuitable. On the contrary, absorbance of the PC phosphor is significantly enhanced compared to that of the bulk phosphor when $\lambda_p = \lambda_1 = 451.6$ nm (the PBE) or $\lambda_p = \lambda_3 = 461.9$ nm (the second PBE), as expected from our earlier discussion. Figure 2-2-5(b) displays how the PL enhancement factor at $\lambda_p = \lambda_1$ (i.e., where the enhancement is maximum) changes as a function of the number of pairs of layers, *N*. The enhancement factor increases monotonically as *N* increases, from 2.6 for $N = 10$ to 6.9 for $N = 30$. This clearly demonstrates that a greatly enhanced PL is attainable by structuring phosphor into a vertical PC and tuning the PBE (preferrably in the HIB) of the vertical PC to the pump wavelength. It should be noted that λ_1 undergoes a blueshift as *N* increases, which is a well-known property of DBRs. Therefore, for each *N* in Fig. 2-2-5(b), the enhancement factor has been determined for a shifted spectral position of λ_1.

So far, we have investigated the case where the pump photons used for phosphor excitation are monochromatic. However, phosphor excitation is typically achieved using a light source with a broad emission bandwidth. For example, standard white LEDs that are commercially available consist of a blue LED with a yellow phosphor cap. The blue LED contributes a blue hue to the overall color and at the same time serves as the excitation source for the yellow phosphor [11]. In order to demonstrate the practical merits of the proposed PC phosphor, it is therefore necessary to investigate the case of phosphor excitation using a light source with a finite emission bandwidth. For this purpose, a Gaussian spectral profile with a full-width at half-maximum (FWHM) bandwidth of 20 nm is assumed.

Shown in Fig. 2-2-6(a) are the absorbance of the vertical PC phosphor and the bulk phosphor, when a pump source is the broad bandwidth light source, as a function of the "peak" wavelength of the gaussian spectral profile. In this case, absorbance $\mathrm{A_{broad}}(\lambda)$ at the peak wavelength of the gaussian pump source λ is given by

$$\mathrm{A_{broad}}(\lambda) = \int_{\lambda-3\sigma}^{\lambda+3\sigma} \mathrm{A_{mono}}(x) \cdot \frac{1}{\sqrt{2\pi}\cdot\sigma} \exp\left[\frac{-(x-\lambda)^2}{2\sigma^2}\right] \mathrm{d}x$$

where $\mathrm{A_{mono}}(\lambda)$ is absorbance when a pump source is a monocromatic source with wavelength λ and σ is the standard deviation, which is called the Gaussian RMS width.

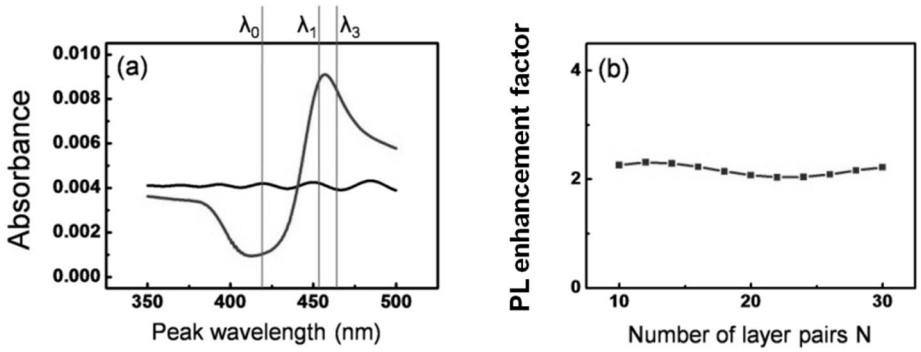

Figure 2-2-6 Phosphor characteristics of the vertical PC phosphor and bulk phosphor when pumped by a broad bandwidth light source. (a) Absorbance spectra of the vertical PC phosphor with $N = 30$ (gray line) and of the bulk phosphor (black line) as a function of the peak wavelength of the broad bandwidth light source. (b) PL enhancement factor of the vertical PC phosphor as a function of the number of pairs of layers in the PC phosphor.

Two major differences between this spectra and that of the previous case using monochromatic light pumping, which is shown in Fig. 2-2-5, should be noted. The first difference is that the maximum absorbance is substantially reduced, which results in a reduction in the absorption enhancement factor. The absorbance peak, however, is broader, which results in a large useful bandwidth for the pump source. The second difference is that the wavelength for maximum absorbance does not coincide with λ_1 and it is redshifted compared to the wavelength from the monochromatic pumping case. While the absorbance reduction is simply due to the fact that a broad bandwidth light source contains photons at wavelengths other than the optimized one ($\lambda = \lambda_1$), the shift in the absorbance peak wavelength can also be explained. Those photons emitted from the broad bandwidth light source with

wavelengths shorter than λ_1 fall in the PBG. Thus, their propagation through the PC phosphor is forbidden and only the phosphor within a short distance from the surface can be excited, which results in a poor excitation efficiency. Consequently, the absorbance peak of pump photons with a gaussian spectral profile is effectively shifted to a wavelength that is longer than λ_1. Nevertheless, the absorbance of the vertical PC phosphor is still much stronger than that of the bulk phosphor. Specifically, the absorbance of the PC phosphor is approximately 2.2 times higher at the absorbance peak of λ = 457 nm (instead of λ_1 = 451.6 nm) than the absorbance of the bulk phosphor. Further, the enhancement in pump photon absorption is preserved over a very broad spectral range of pump wavelengths ($\Delta\lambda \sim$ 50 nm). This implies a large tolerance in wavelength tuning between the peak wavelength of the broad bandwidth pump source and the PBE of the PC phosphor, which is extremely important if the vertical PC phosphor is to be considered for use in white LEDs.

Figure 2-2-6(b) is the PL enhancement factor when pumped by the broad bandwidth light source, shown as a function of the number of pairs of layers in the PC. For each value of *N*, the enhancement factor is estimated at the peak absorbance wavelength. Unlike the case of a monochromatic pump source, the absorption enhancement factor varies little with the number of pairs of layers in the phosphor, due to the broadness of the absorbance spectrum. In other words, the characteristics of the vertical PC phosphor are not sensitive to the number of pairs of layers when a broad bandwidth pump source is used for phosphor excitation. We have shown the simulation results only for the layer pair numbers larger than 10, because the photonic band structure of the PC and therefore the PBE identification becomes obscure progressively as the pair number gets smaller. In addition, the absorbance

peak shifts significantly for small N so that deduced enhancement factor loses its relevance. According to Fig. 2-2-6(b), 10 pairs of layers would be as efficient as 20 or even 30 pairs of layers in terms of the phosphor excitation efficiency, which apparently has a big impact on real applications, such as shorter processing time and higher fabrication yield at the end.

2.3 Sample Design and Fabrication

In this session, I chose polymer materials to fabricate the proposed vertical PC phosphor structure, because of their capacity to easily form multiple layer stacks by the spin-coating method. Specifically, we employed poly n-vinylcarbazole (PVK) and cellulose acetate (CA) as the high and low refractive index materials, respectively. According to our own spectroscopic ellipsometry measurements, their respective refractive indices were about 1.7 and 1.5 at a wavelength of $\lambda \sim 450$ nm, as shown in Figs. 2-3-1(a) and (b), while their extinction coefficients were negligibly small. The chosen pair of polymer materials displays a sizable difference in refractive index, ~0.2, which is a prerequisite for the resultant PC to exhibit distinct band structure anomalies, such as PBG and PBEs. Moreover, the PVK and CA were dissolved in different solvents, so that they were not intermixed while being stacked on top of each other by spin-coating [12,13], which is of great importance regarding fabrication. Prior to the spin-coating process, CdSe/ZnS core-shell QDs were dispersed in PVK to make only the high refractive index layers optically active. Figure 2-3-1(c) displays extinction coefficient, or imaginary part of refractive index, of CdSe/ZnS QDs embedded in the PVK solution, which is also measured by ellipsometry. As we explained previously, the electric field intensity of the incident pump beam is periodically modulated within the PC phosphor structure, so that its local maxima coincide with the high/low refractive index layers when the photon energy was tuned to the PBE in the high/low index band (HIB/LIB). Therefore, the presence of fluorescent agents in only one kind of layers is sufficient, depending on which PBE mode is utilized.

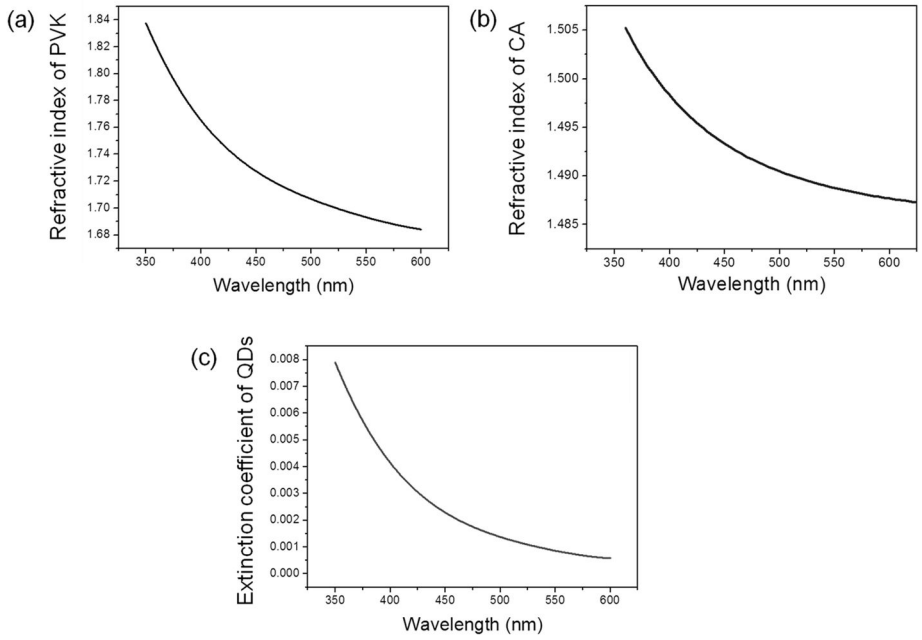

Figure 2-3-1 Refractive indices of (a) PVK and (b) CA and (c) extinction coefficeint of CdSe/ZnS QDs embedded in PVK solution.

2.3.1 Sample design

I considered three model phosphor structures, one "*bulk*" and two vertical PC structures, "*bulk-like PC*" and "*PC*". In terms of structure, the three phosphor structures differ only in the thicknesses of their low refractive index CA layers: d_L = 0 nm for the bulk, 40 nm for the bulk-like PC, and 62 nm for the PC, respectively. However, the high index PVK layer thicknesses were equal for all three phosphor structures: d_H = 64 nm. The total number of layer pairs was also fixed at N = 15. These structural conditions infer that the accumulated total thickness of the high index layers ($d_H \times N$ = 960 nm), and thus the number of QDs, remained the same for all three types of phosphor structures, regardless of the QD concentration in PVK. Table 2-3-1 compares three types of modelled phosphor structures. It is worth mentioning that the bulk phosphor was simply a single thick PVK layer, while the bulk-like PC phosphor had a CA layer thickness significantly detuned (from that of the PC phosphor); therefore, neither of them would have any well-defined PBE modes in the frequency range of interest.

All the phosphor structures were assumed to be prepared on a transparent quartz substrate with refractive index and thickness of $n_{QZ} \sim 1.54$ and 1000 μm, respectively. Figure 2-3-2(a) shows the calculated reflectance spectra of the three phosphor structures. The PC phosphor structure exhibits the well-defined first reflectance minimum on the long-wavelength side of the stop band, λ_{+1}, which corresponds to the PBE in the HIB of the ideal PC. In contrast, the reflectance spectra for both the bulk and the bulk-like phosphor structures have no distinct band related features, only Fabry-Perot oscillations with shallow modulation depths. It should be mentioned that the reflectance spectrum for the bulk-like phosphor is very similar to that of the bulk phosphor, which explains the term "bulk-like."

	d_H (nm)	**d_L (nm)**	PBG region
PC	64	**62**	Violet (400 ~ 440 nm)
Bulk-like PC	64	**40**	UV (below 400 nm)
Reference	64	**0**	

Table 2-3-1 Comparison between three types of modelled phosphor structures.

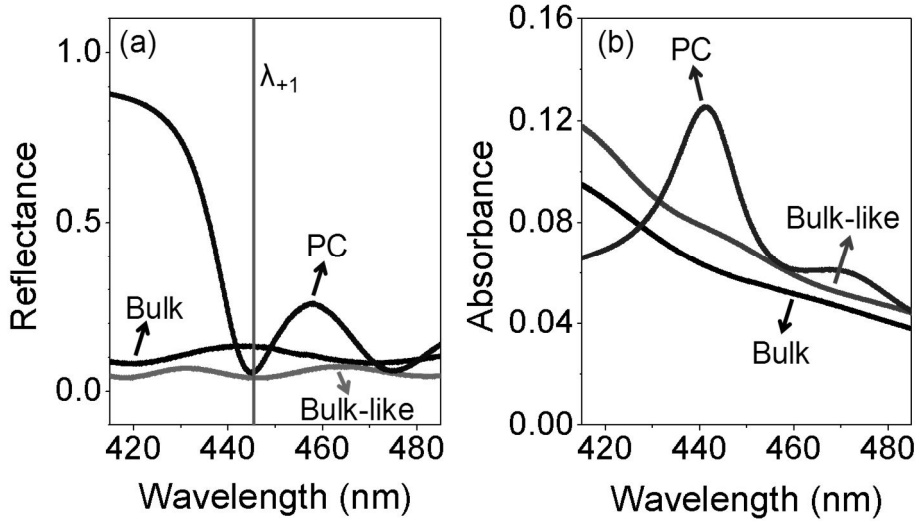

Figure 2-3-2 (a) Calculated reflectance spectra of three model phosphor structures: bulk, bulk-like PC, and PC phosphors. (b) Calculated absorbance spectra of the three model phosphor structures.

Figure 2-3-2(b) shows the absorbance spectra calculated for the three types of phosphor structures. The absorbance spectrum of the PC phosphor structure displays a peak at approximately λ_{+1}, which is exactly what we anticipated. However, there is no noticeable peak in the absorption spectra of the bulk and the bulk-like PC phosphors, which is essentially due to the lack of any distinct photonic band structure effects. The gradual increase in absorbance as the wavelength becomes short is a simple reflection of the dispersive nature of QDs, having nothing to do with any resonant absorption of pump photons. Comparing the values at λ_{+1}, the PC phosphor has the largest absorbance, which is approximately twice that of the bulk phosphor. It is obvious that absorption enhancement should result in an increase in fluorescence. We therefore expect largely improved fluorescence when the pump photon energy is tuned to the PBE mode of the PC phosphor structure.

2.3.2 Fabrication method

It should be mentioned that the bulk phosphor, which would serve as a reference, could not be constructed by the spin-coating method. The viscosity of the PVK:QD solution was too low to produce a 960-nm-thick film by a single spin-coating process, while efforts for multiple spin-coatings failed; a fully cured underlying layer would immediately dissolve when over-coating with a new layer, in an attempt to thicken the film. Thus, the bulk-like phosphor structure plays an important role: it behaves like a bulk phosphor, in the sense that it has neither PBG nor PBEs in the spectral region of interest—Fig. 2-3-2(a); yet it can be constructed by multiple spin-coating processes, like the PC phosphor

Three kinds of multi-film phosphor structures were fabricated by alternately spin-coating two kinds of polymer materials: PVK and CA for the high and low refractive index layers, respectively. For the preparation of the high index polymer with fluorescing ability, PVK (Sigma Aldrich, USA) was dissolved in toluene at the concentration of 18 mg/ml, followed by dispersing CdSe/ZnS QDs (QD Solution, Korea) to the concentration of 0.67 mg/ml. The QD concentration corresponds to 1.67 mM in molar concentration, which is within the safe limit that does not damage the photonic band structure of the resultant PC. For the low index polymer, CA (Sigma Aldrich) was dissolved in diacetone alcohol in two different concentrations: 18 mg/ml for the PC phosphor and 12 mg/ml for the bulk-like phosphor. All the concentrations were carefully pre-calibrated and determined to obtain the desired thicknesses when spin-coated at a fixed spin speed of 4,000 rpm. After each spin-coating process, the sample was cured on a hot plate at 80°C for 5 minutes. The PVK:QD layers and the CA layers were alternately spin-coated up to 15 layer pairs on a quartz substrate to complete the PC phosphor structures.

I can assure the polymer thin films and phosphor structures have exact thicknesses as intended by measuring the reflectance spectrum (indirect method) and getting SEM images (direct method).

To measure the reflectance spectrum of fabricated phosphor structures, I employed a simple home-made micro-reflectance measurement setup based on a 1×2 fiber coupler [14]. The 1×2 fiber coupler enables to feed white light to the sample and simultaneously to capture signal reflected from the sample using a single butt-end fiber tip, greatly simplifying the conventional reflectance measurement setup. A tungsten halogen lamp was used as a white light source, and optical signal reflected from sample was directly fed into an optical spectrum analyzer through a fiber

Figure 2-3-3(a) shows a cross-sectional scanning electron microscope (SEM) image of a fabricated PC phosphor. The identification of the individual layer thicknesses is difficult, owing to the electric charging effect, as well as the partial damage and distortion generated when breaking the sample in preparation for the imaging of the cross-sectional surface. However, the image is sufficiently clear to confirm that multiple layers were stacked alternately and uniformly.

Figures 2-3-3(b) and (c) display the measured reflectance spectra for the PC and the bulk-like phosphor structures, in comparison with the corresponding calculated ones. The agreement between the measured and calculated results is excellent, providing indirect but decisive evidence that the phosphor structures were successfully realized as designed. In fact, it is from these reflectance spectrum fittings that we determined the layer thicknesses in the PC phosphor: d_H = 64 nm and d_L = 62 nm. It needs to be reminded that the QD concentration in the PVK layers was intentionally kept low (< 10 mM), so that the optical absorption by the

QDs remained insignificant, which was necessary to ensure that the PC structures retained their band-structure related properties. This condition allows us to make comparisons between theory and experiments, and thus evaluate the structural quality and performance characteristics of the fabricated PC phosphors. The insets embedded in the figure are photographic images taken for the corresponding phosphor structures under normal daylight conditions. The PC phosphor structure exhibits a relatively strong blue hue, while the bulk-like phosphor is gray, and both images are in good accordance with the corresponding reflectance spectra.

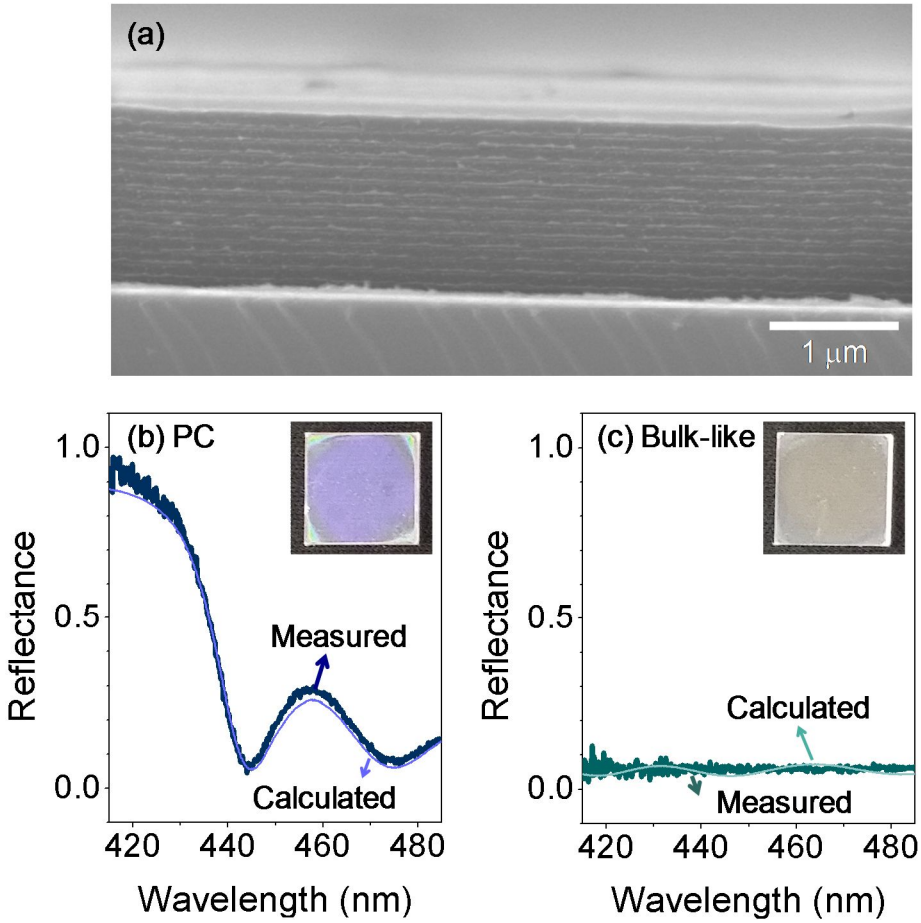

Figure 2-3-3 (a) Cross-sectional SEM image taken for a 1D PC phosphor structure, fabricated by the multiple spin-coating method. Measured and calculated reflectance spectra of: (b) the PC phosphor and (c) the bulk-like phosphor. The insets in (b) and (c) are photographic images for the corresponding phosphor structures.

2.4 Measurement and Analyses

2.4.1 Measurement setup

In order to characterize the vertical PC phosphors, an experimental setup to measure PL intensity as a function of pump wavelength was required. Figure 2-3-3 shows the PL measurement setup with a wavelength-selectable monochromatic light source to characterize PL intensity from phosphor structures. A broadband xenon lamp was combined with a monochromator to build a wavelength-tunable pump source across a wide spectral range with a narrow linewidth, yet delivering pump intensity strong enough to optically excite the phosphor samples. The spectral linewidth of the tunable pump source was set to 2 nm at full-width at half-maximum (FWHM), which is sufficiently narrow to resolve any detailed spectral feature appearing in the reflectance spectra. The phosphor samples were pumped at normal incidence, while the fluorescence emitted from the QDs through the quartz substrate was directed to a spectrometer. All the PL measurements were made at room temperature.

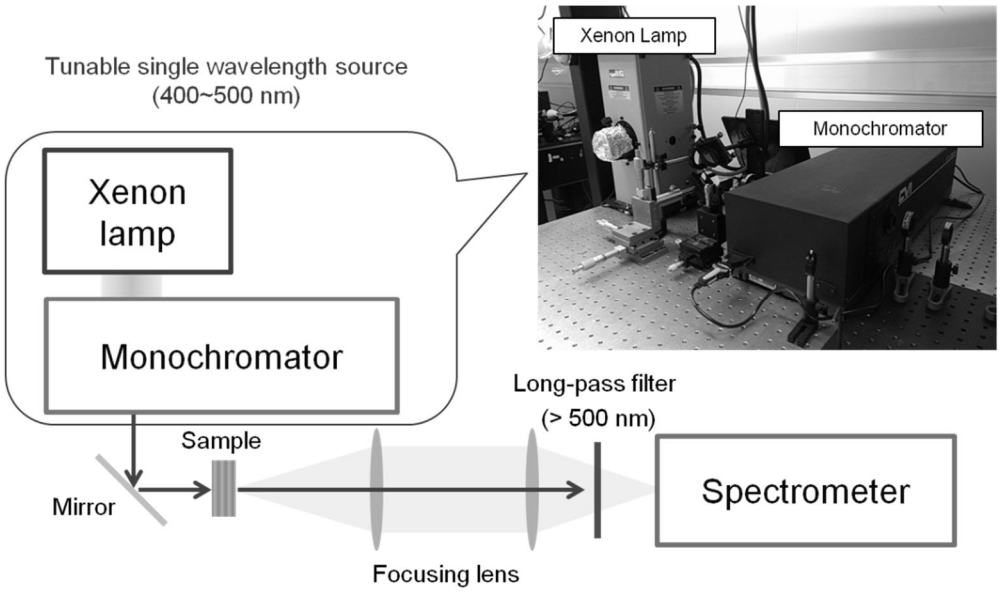

Figure 2-4-1 PL measurement setup with a wavelength-tunable monochromatic light source to characterize PL intensity from phosphor structures.

2.4.2 Photoluminescence spectra

Figures 2-4-2(a) and 2-4-2(b) show the PL spectra measured for the PC and the bulk-like phosphor structures, respectively. Here we only present PL spectra selected for certain representative pump wavelengths. Regardless of the pump wavelengths, PL spectra remain unchanged in terms of their peak wavelengths (~580 nm), as well as spectral linewidths (~35 nm in FWHM). As the pump wavelength changes, however, the peak intensity varies considerably, especially for the PC phosphor.

In order to account for the intensity variation of the pump beam, we also measured the pump beam spectra while scanning the monochromator across the wavelength range of interest—Fig. 2-4-3(a). The measurements were made every 5 nm, except for the important wavelength region near λ_{+1} (420 nm < λ_{pump} < 460 nm), where the measurements were made in 2-nm steps. The PL intensity is plotted in Fig. 2-4-3(b) as a function of pump wavelength, where each data point is obtained by dividing the maximum PL intensity in Figs. 2-4-2(a) and 5(b) by the pump beam intensity measured at the corresponding pump wavelength.

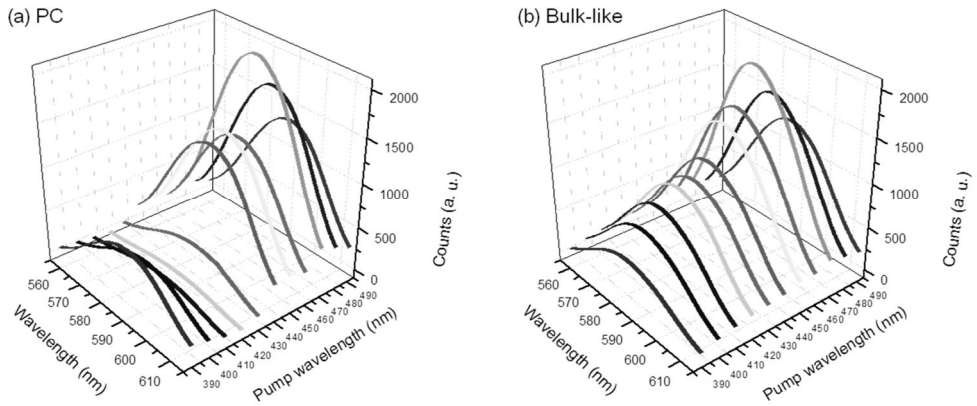

Figure 2-4-2 PL spectra measured as a function of pump wavelength: (a) the vertical PC phosphor and (b) the bulk-like phosphor.

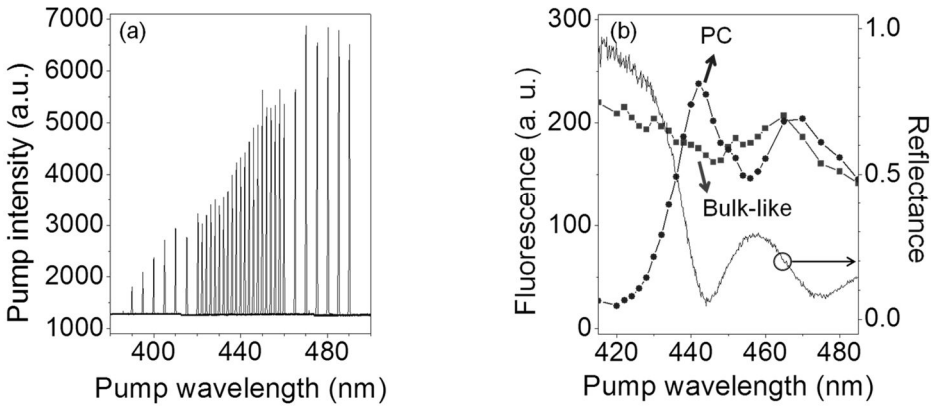

Figure 2-4-3 (a) Pump beam spectra taken while the monochromator is scanned. (b) PL intensity plotted as a function of pump wavelength, after normalization with the pump intensity, for both the PC and bulk-like phosphors. The measured reflectance spectrum of the PC phosphor is also shown as a spectral reference.

It can be seen in Fig. 2-4-3(b) that the PL intensity from the PC phosphor changes drastically as the pump wavelength increases, whereas the bulk-like phosphor exhibits only a small variation. More importantly, the fluorescence strength variation for the PC phosphor is in accordance with the reflectance spectrum, which is also shown in the figure: the PL maxima coincide with the reflectance minima. Essentially, the figure highlights the correlation between fluorescence strength and photonic band structure, which agrees with our initial assessment that the fluorescence from the PC phosphor structure can be improved when the pump photon energy is tuned to the wavelength of the reflectance minimum (or the PBE of the PC with an infinite translational symmetry).

2.4.3 Photoluminescence enhancement factor

I estimated the PL enhancement factor by considering the PL intensity ratio of the PC phosphor to that of the bulk-like phosphor, which is shown in Fig. 2-4-4(a). The PL enhancement factor provides a means of evaluating the effect in a quantitative manner: the enhancement factor reaches its maximum value of ~1.36 when $\lambda_{pump} \sim \lambda_{+1}$. For a direct comparison, we also show the theoretically calculated absorption enhancement factor in Fig. 2-4-4(a), which is derived from the ratio between the calculated absorbance of the vertical PC and bulk-like phosphor structures—Fig. 2-3-1(b). The calculated absorbance enhancement factor depicts quite well the overall PL enhancement factor determined experimentally. The close resemblance of the two curves confirms our notion that the PL intensity is proportional to the degree of pump photon absorption by phosphor. However, their absolute enhancement factor values differ: 1.36 (PL enhancement; experiment) versus 1.60 (absorption enhancement; theory). We attribute this difference mainly to the fact that the actual structure could never be identical to the ideally designed one. The discrepancy could be also partially due to any physical mechanisms that hamper fluorescent photons from escaping the structure, such as internal reflection, lateral guiding, and random scatterings. In addition, the IQE of QDs that mediates between absorption and emission may be dispersive, which might be an explanation for the wavelength-dependent discrepancy in the enhancement factors. Although not demonstrated in this session, the enhancement factor could be further improved by increasing the number of layer pairs, but with a penalty in narrowing down the useful bandwidth of pump wavelengths, as indicated in previous session 2.2 in this thesis.

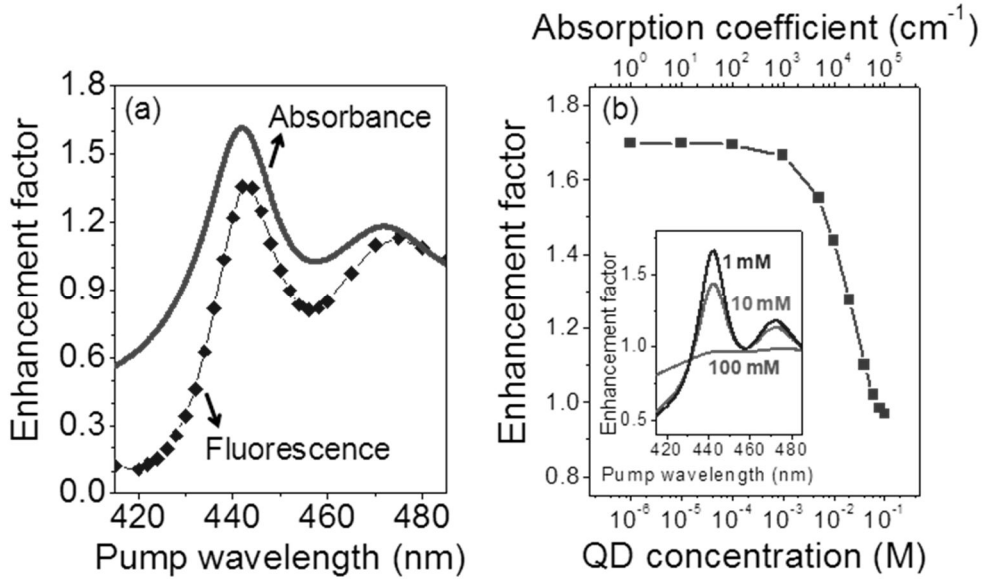

Figure 2-4-4 (a) Enhancement factor of the vertical PC over the bulk-like phosphor versus pump wavelength in both fluorescence (experimental) and absorption (theoretical). (b) Calculated absorption enhancement factor as a function of QD concentration. The QD concentration is expressed in terms of absorption coefficient, as well as molar concentration. The inset shows the calculated absorption enhancement factors for the QD concentrations of 1 mM, 10 mM, and 100 mM, presented as a function of pump wavelength.

As an assessment of the QD concentration range that can be meaningful for the present purpose, I performed theoretical evaluations for a wide range of QD concentrations. Figure 2-4-4(b) shows the calculated absorption enhancement factor as a function of QD concentration; the QD concentration (in M) is also expressed in terms of the absorption coefficient (in cm^{-1}), using the molar absorption coefficient equation in the literature [15]. As seen in the figure, the enhancement factor below the QD concentration of 1 mM saturates quickly to ~1.7, which therefore becomes the maximum achievable enhancement factor. On the other hand, the enhancement factor rapidly decreases when the QD concentration exceeds 1 mM, reaching the null effect (or 1 in the enhancement factor) at the QD concentration of ~70 mM. In fact, as the QD concentration approaches the null effect point, the PC band structure vanishes, as shown in the inset of Fig. 2-4-4(b), where the pump wavelength dependent absorption enhancement factor is plotted for three QD concentrations, 1 mM, 10 mM, and 100 mM.

2.5 Summary

The validity of the concept of vertical PC phosphors for efficient optical pumping has been explored. Calculations determined that when photons of a PBE mode are incident onto a periodically stacked vertical PC structure, the optical field builds up resonantly inside the structure, offering an opportunity to largely improve the optical interaction with the material. Consequently, if an optically active agent is introduced into such a structure, the absorption of incident photons can be maximized when the photon energy is tuned to a PBE.

Following the initial theoretical modelling, I realized the corresponding nano-engineered phosphor structure by alternately stacking two kinds of polymer materials, PVK:QD and CA, up to 15 layer pairs by the spin-coating method. CdSe/ZnS core-shell QDs were dispersed in PVK, so that only the high refractive index layers could fluoresce. The reflectance spectrum measured for the resultant 1D PC phosphor structure exhibited well-defined band structure properties, including the stop band. The fluorescence spectrum was measured as a function of pump wavelength. As anticipated from the theoretical calculations, the fluorescence intensity became highest when the pump photon energy coincided with the first reflectance minimum λ_{+1}, which is a PBE of the corresponding PC with a finite number of layer pairs. In comparison with a reference phosphor, the PL intensity from the PC phosphor was improved by a factor of 1.36.

Although there is limitation in concentration of QDs embedded in the vertical PC phosphor structures, I proved the idea of PC phosphors successfully and I will suggest another kind of PC phosphors to make up for the weakness of the vertical PC phosphors.

References

[1] K. Min, Y.-K. Choi, and H. Jeon, "Model calculations for enhanced fluorescence in photonic crystal phosphor," Opt. Express **20**, 2452-2459 (2012).

[2] K. Min, S. Choi, Y. Choi, and H. Jeon, "Enhanced fluorescence from CdSe/ZnS quantum dot nanophosphors embedded in one-dimensional photonic crystal backbone structure," Nanoscale **6**, 14531-14537 (2014).

[3] John D. Joannopoulos, Robert D. Meade, and Joshua N. Winn, *Photonic crystals: Molding the flow of light* (Princeton University Press 2008).

[4] P. Yeh, *Optical Waves in Layered Media* (Wiley 1988)

[5] S. L. Chuang, *Physics of Photonic Devices, 2nd ed.* (Wiley 2009).

[6] S. Y. Lin, J. G. Fleming, Z. Y. Li, I. El-Kady, R. Biswas, and K. M. Ho, "Origin of absorption enhancement in a tungsten, three-dimensional photonic crystal," J. Opt. Soc. Am. B **20**, 1538-1541 (2003).

[7] Y. Liu, C. Jiang, Y. Lin, and W. Xu, "Slow-light enhancement of stimulated emission of atomic systems in photonic crystals," J. Opt. Soc. Am. B **27**, 442-446 (2010).

[8] C. M. Johnson, P. J. Reece, and G. J. Conibeer, "Slow-light-enhanced upconversion for photovoltaic applications in one-dimensional photonic crystals," Opt. Lett. **36**, 3990-3992 (2011).

[9] A. R. Kortan, R. Hull, R. L. Opila, M. G. Bawendi, M. L. Steigerwald, P. J. Carroll, and L. E. Brus, "Nucleation and growth of CdSe on ZnS quantum crystallite seeds, and vice versa, in inverse micelle media," J. Am. Chem. Soc. **112**, 1327-1332 (1990).

[10] D. Gerion, F. Pinaud, S. C. Williams, W. J. Parak, D. Zanchet, S. Weiss, and A. Paul Alivisatos, "Synthesis and properties of biocompatible water-soluble silica-coated CdSe/ZnS semiconductor quantum dots," J. Phys. Chem. B **105**, 8861-8871 (2001).

[11] K. Bando, K. Sakano, Y. Noguchi, and Y. Shimizu, "Development of high-bright and pure-white LED lamps," J. Light Vis. Environ. **22**, 2-5 (1998).

[12] T. Komikado, A. Inoue, K. Masuda, T. Ando, and S. Umegaki, "Multi-layered mirrors fabricated by spin-coating organic polymers," Thin Solid Films, **515**, 3887-3892 (2007).

[13] V. M. Menon, M. Luberto, N. V. Valappil, and S. Chatterjee, "Lasing from InGaP quantum dots in a spin-coated flexible microcavity," Opt. Express, **16**, 19535-19540 (2008).

[14] Y. Park, J.-S. Choe, and H. Jeon, "Design, fabrication, and micro-reflectance measurement of a GaAs/AlAs-oxide antireflection film," J. Kor. Phys. Soc., **40**, 245-249 (2002).

[15] D. F. Swinehart, "The Beer-Lambert Law," J. Chem. Educ., **39**, 333 (1962).

Chapter 3

Lateral Photonic Crystal Phosphor

3.1 Introduction

I explored the PBE effect in the vertical PC phosphors theoretically and experimentally both, however we may have difficulty in applying vertical PCs to real optical devices due to their limit in concentration of phosphor materials. [1]

Figure 3-1-1 displays schematics of the vertical PC phosphor and the lateral PC phosphor and we can see that there are differences in distance from the pump source between each phosphor layers because pump photon propagation is parallel to the direction of periodicity of the vertical PC. Consequently, phosphor layers at a long distance from the source are less pumped and we cannot ensure the PBE effect and PL enhancement any more.

On the other hand, in lateral PC structures, all phosphor regions are equidistant from the pump source and pumped on the same and I expected that the PBE effect is valid in high concentration of phosphors, e.g., QDs. This is our motivation to develop the lateral PC phosphors.

Outside of that, the lateral thin-film PC structures have unique photonic properties at various symmetry points in *k*-vector space. Especially I paid attention to the *Γ-point* PBE, which the lateral component of wave vector **k** does not exist. Because the direction of the wave vectors at Γ-point PBEs should be normal to the surface, various surface-emitting laser devices using Γ-point PBE effects have been

developed [2-4]. I applied the Γ-point PBE effects in the opposite way from PBE lasers and attempted to excite resonant PBE modes by normally incident pump photons.

There are various patterning methods to construct the lateral PC, for example, electron beam lithography, photo lithography, and laser holographic lithography (LHL). After patterning on the thin films as slab waveguides, dry or west etch processes are performed to fabricate thin-film photonic crystal structures. Table 3-1-1 shows comparison between three common lithography methods. Because the PC phosphors are designed for light-emitting devices, we need a patterning method for large areas in sub-micron scale. Electron-beam lithography offers very high spatial resolution but it is often a tedious and expensive process for large area patterning. Using an opaque plate as a photomask, patterns are written in large area quickly but its spatial resolution is lower than that of other lithography method. Accordingly, I employed LH lithography to fabricate the lateral PC phosphors.

Similarly to the logical process of chapter 2, I will model the lateral PC phosphor structures theoretically at first. Next, electric field profiles within the PC structure and PBE effects will be explored using the FDTD numerical method [5]. Finally 1D lateral PC phosphors will be fabricated and investigated. The reason why I explored the 1D structure is that the PBE effect of the 1D lateral PCs depends on polarization of the pump source, which will be discussed in chapter 3.4.

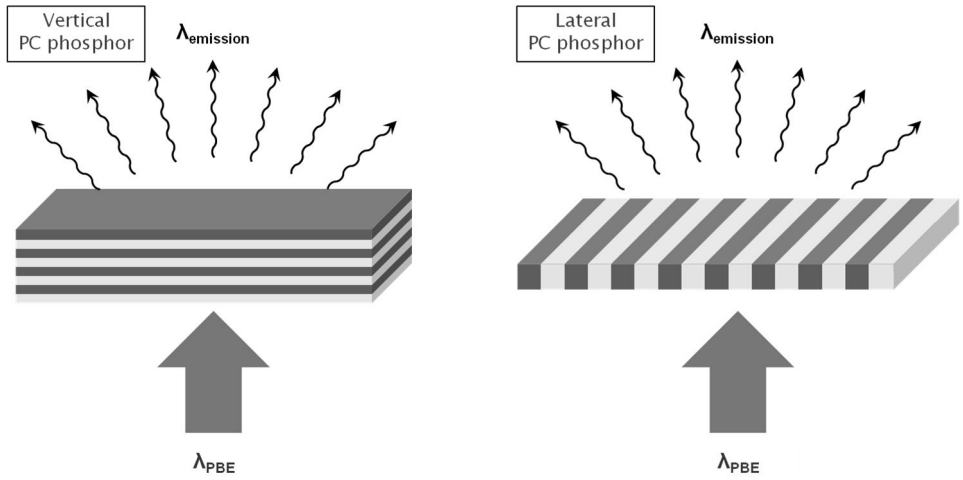

Figure 3-1-1 Schematics of the vertical PC phosphor and the lateral PC phosphor.

	E-beam lithography	**Photo-lithography**	**LH lithography**
Cost	high	high	low
Throughput	low	high	high
Large-area	X	O	O
Mask	O	O	X
Minimum feature size	~ 10 nm	~ few μm	~ 100 nm
Applicability	O	O	X (only periodic patterns)

Table 3-1-1 Comparison between three common lithography methods.

3.2 Model Calculation

I performed numerical analyses about lateral PC structures using the FDTD method. Photonic band structures of the lateral PCs were constructed and electric field localizations at the various PBE modes in the lateral PC slabs were probed. On the assumption that the IQE of the phosphor is unity, as we supposed in chapter 2, absorbance of pump photons in the lateral PC phosphor was calculated.

The lateral 1D PC phosphor structure considered in chapter 3.2 consists of two materials which refractive indices are n_L = 1.8 (for low index materials) and n_H = 2.0 (for high index materials), which are the typical refractive indices of CdSe/ZnS QDs and silicon nitride, respectively. Figure 3-2-1(a) shows a schematic of the lateral PC phosphor structure. The period of the structure is given by a = 300 nm and filling factor of QDs in each period is 50 %, which means $d_H = d_L$ = 150 nm. Unlike the vertical PC structures, the lateral PC structures do not have periodicity in normal direction to surface. Therefore, the PWE method is not suitable to investigate photonic band structures of lateral PCs.

The FDTD simulation in unit cell of the lateral PC structure, which is shown in Fig. 3-2-1(b), was performed to calculate the band structure, electric field profiles of PBE modes, and absorbance spectra. In the unit cell, I set the x-axis parallel to direction of the periodicity and the z-axis is the vertical axis to surface.

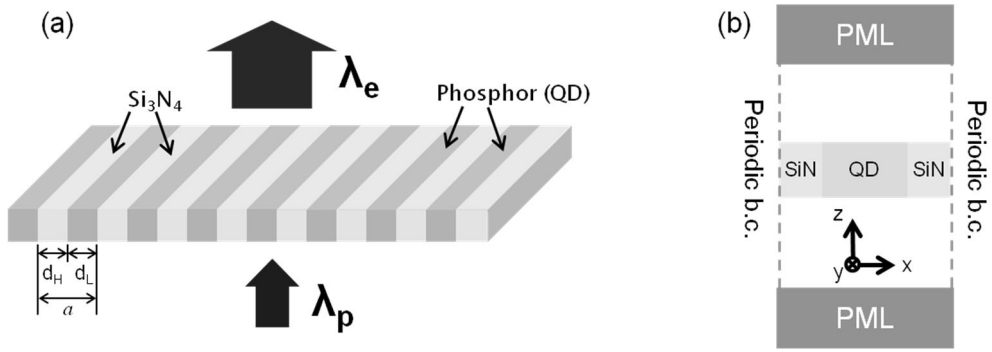

Figure 3-2-1 (a) A schematic of the lateral 1D PC phosphor structure consisting of silicon nitride and QDs. (b) Unit cell of the lateral 1D PC structure, in which FDTD simulations are performed to calculate photonic properties of the lateral 1D PC.

3.2.1 Photonic band-edge modes of lateral 1D photonic crystals

We first examined the photonic band structure of the lateral 1D PC structure utilizing the FDTD method. The band structure we obtained is common dispersion relation of photons in 1D PCs, which have lateral periodicity or vertical periodicity either. And there are two symmetric points in the lateral 1D PC, in case of $k_x = 0$ and $k_x \neq 0$, where k_x is the wave vector in direction of periodicity. Figure 3-2-2 shows the photonic band structure of the lateral 1D PC and corresponding electric field profiles of PBE modes in both cases. In every PBE modes I simulated, electric fields confined in the lateral PC phosphor slab and it seems that PL enhancement effects at PBE wavelengths are valid.

However, an important factor for efficient pumping is not only confinement of electric fields at PBEs but also degree of coupling of external pump photons and PBE modes. We knew intuitively which PBE mode is suitable to be excited by the external source among the case of $k_x = 0$ and $k_x \neq 0$. Figure 3-2-3 displays directions of wave vector **k** of PBE modes at each symmetric point. In case of $k_x \neq 0$, direction of vector **k** is vertical to propagation direction of pump photons and there is no excitation of photonic modes. On the other hand, in case of $k_x = 0$, wave vector **k** and propagation of pump photons head in the same direction and coupling of external pump photons and PBE modes will occur.

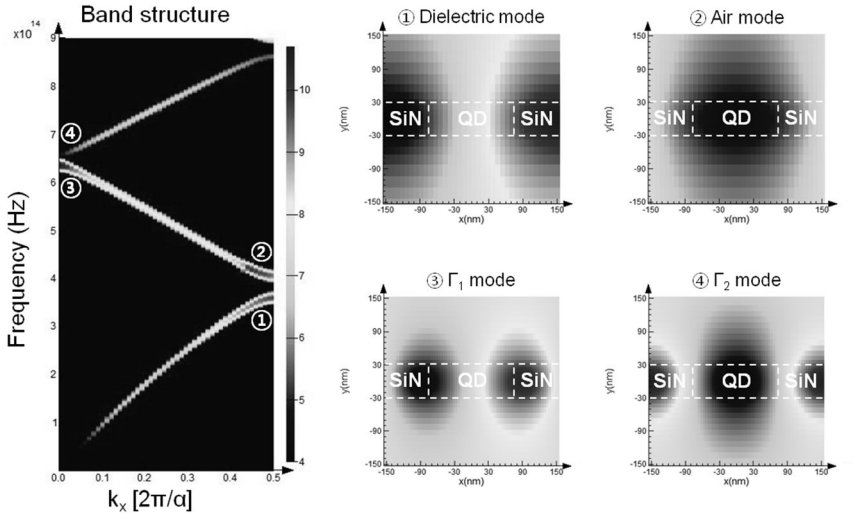

Figure 3-2-2 The photonic band structure of the lateral 1D PC and corresponding electric field profiles of PBE modes in case of $k_x \neq 0$ (①,②) and $k_x = 0$ (③,④).

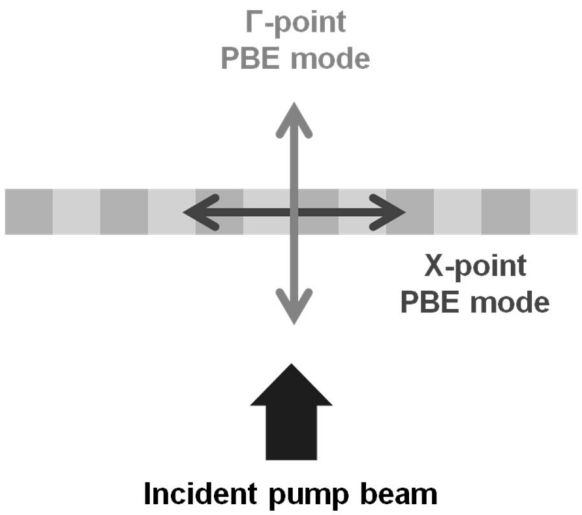

Figure 3-2-3 Directions of wave vector **k** of PBE modes at each symmetric point

I called the symmetric point with $k_x = 0$ to *Γ-point* because Γ-point used to mean the symmetric point with none lateral component of the wave vector in the slab waveguide generally [6].

The lateral 1D PC phosphor structures will be prepared on a quartz substrate with refractive index of $n_{QZ} \sim 1.54$ so that some FDTD simulation processes repeated. As shown in Fig. 3-2-4, the photonic band structure of the lateral 1D PC with a substrate resemble that of the lateral 1D PC without a substrate except narrowing of the PBG width due to change of the effective refractive index of the structure. Because index difference between a quartz substrate and a lateral PC slab is smaller than that between air and a PC slab, a shape of the electric field profile at Γ-point PBE wavelengths in the PC slab near a quartz substrate looks somewhat leaky but well confined as ever.

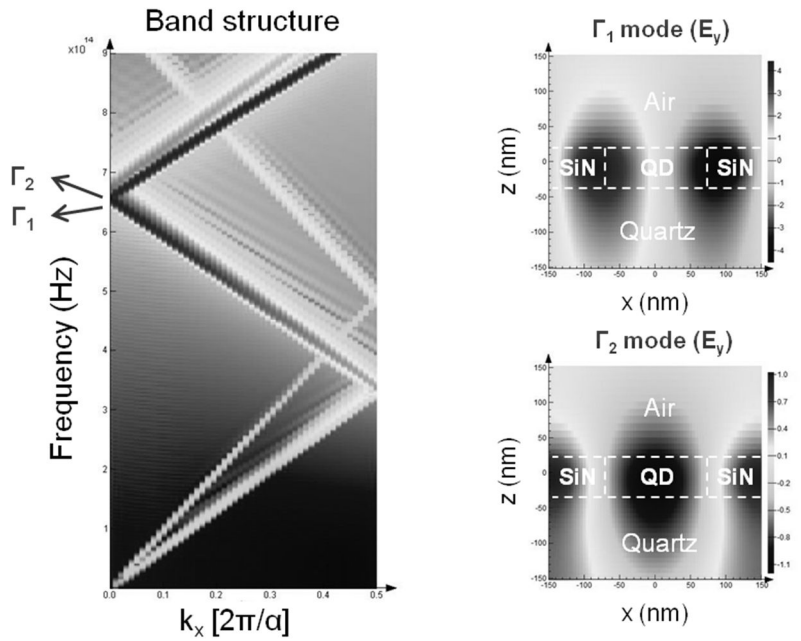

Figure 3-2-4 The photonic band structure of the lateral 1D PC with a quartz substrate and corresponding electric field profiles of the Γ-point PBE modes.

3.2.2 Absorption enhancement

We now evaluate PL enhancement at Γ-point PBE in the lateral 1D PC phosphor by calculating absorbance of pump photons in the PC structure with an assumption that the IQE of phosphor materials is unity, which is a constant proposition through this thesis. Absorbance per unit volume which can be obtained from the divergence of the Poynting vector [7] is given by

$$\text{Absorbance} = -\frac{1}{2}\cdot \text{real}\left(\vec{\nabla}\cdot\vec{P}\right),$$

which formula is equivalent to

$$\text{Absorbance} = -\frac{1}{2}\cdot \text{real}\left(i\omega\vec{E}\cdot\vec{D}\right).$$

With more simplifications, we get the results suitable for simulation

$$\text{Absorbance} = -\frac{1}{2}\cdot \omega|E|^2\text{imag}(\varepsilon).$$

These processes and results are provided in the commercially available computer software product I used in this chapter, Lumerical FDTD solutions [5]. Figure 3-2-5 shows unit cells of the lateral 1D PC phosphor with the quartz substrate and simple QDs thin film on the quartz for the reference phosphor.

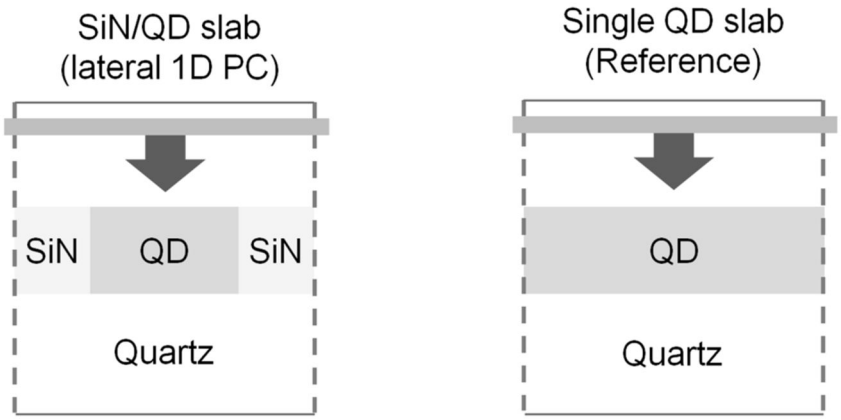

Figure 3-2-5 Unit cells of the lateral 1D PC phosphor with the quartz substrate (left) and simple QDs thin film on the quartz for the reference phosphor (right).

Figure 3-2-6(a) compares the absorbance of the lateral 1D PC phosphor with that of the reference phosphor as a function of the pump photon wavelength when extinction coefficient of phosphor $\kappa_{phosphor}$ is 0.005. It should be noted that simulations in this chapter were performed with *constant* extinction coefficient $\kappa_{phosphor}$ (independent of excitation wavelengths) for the purpose of investigating the PBE effect and absorption enhancement as $\kappa_{phosphor}$ increases. At Γ–point PBEs near the second PBG, two absorbance peaks, which represent Γ_1 PBE and Γ_2 PBE respectively, appear noticeably in the lateral PC phosphor and the values of absorbance are several times larger than that in the reference bulk. This clearly indicates that a greatly enhanced PL is expected by structuring phosphor into a lateral PC and tuning the Γ–point PBE of the lateral PC to the pump wavelength. Figure 3-2-6(b) displays the enhancement factor in PL (or absorbance of pump photons) deduced from the absorbance ratio between the lateral PC phosphor and its bulk counterpart.

I also investigated whether Γ–point PBE effect and absorption enhancement are valid with high concentration of QDs in the lateral PC phosphor. Figures 3-2-7 (a), (b), and (c) show absorbance spectra of pump photons in the lateral PC phosphors with extinction coefficient $\kappa_{phosphor}$ = 0.005, 0.01, and 0.03, respectively. We could recognize two separated absorption peaks clearly when the extinction coefficient of the phosphor is low. Meanwhile, as shown in Fig. 3-2-7(c), a broad absorption peak appears even when the extinction coefficient is 10 times larger than limitation of that of the vertical PC phosphors. No wonder we could not distinguish two PBE peaks as the extinction coefficient increases and a bandwidth of each peak becomes broader.

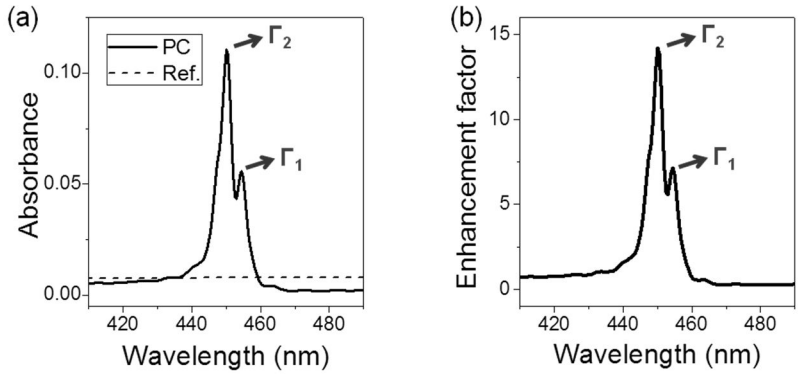

Figure 3-2-6 (a) Absorbance spectra of pump photons in the lateral 1D PC phosphor and the reference phosphor as a function of the pump photon wavelength when extinction coefficient of phosphor $\kappa_{phosphor}$ is 0.005. (b) Enhancement factor in PL (or absorbance of pump photons) of the lateral 1D PC phosphor.

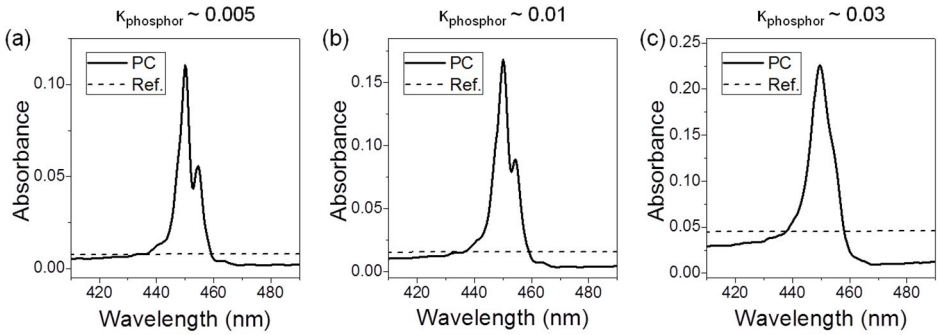

Figure 3-2-7 Absorbance spectra of pump photons in the lateral 1D PC phosphors and the reference phosphors with extinction coefficient $\kappa_{phosphor}$ = 0.005, 0.01, and 0.03 (from left to right).

3.3 Sample Fabrication

3.3.1 Laser holographic lithography

Laser holographic lithography (LHL) is a lithography technique for large area patterning in sub-micron length scale. The basic principle of LH lithography is very similar to in interferometer. In our setup for LH lithography, shown in Fig. 3-3-1(a), electromagnetic waves emitted from a 266-nm diode-pumped solid-state (DPSS) laser propagate are divided into two ways by an objective lens and two coherent lights propagate a long distance to a sample stage. Then the interference pattern occurs as can be seen in Fig. 3-3-1(b), which consists of a periodic series of fringes representing intensity maxima and minima. After post-exposure process, a photoresist (PR) pattern corresponding to the periodic intensity pattern comes out. The period of the periodic pattern is given by

$$\text{Period} = \frac{\lambda}{2\sin\theta}$$

where λ is the laser wavelength (= 266 nm) and θ is the incident angle of photons radiated from the laser source [8].

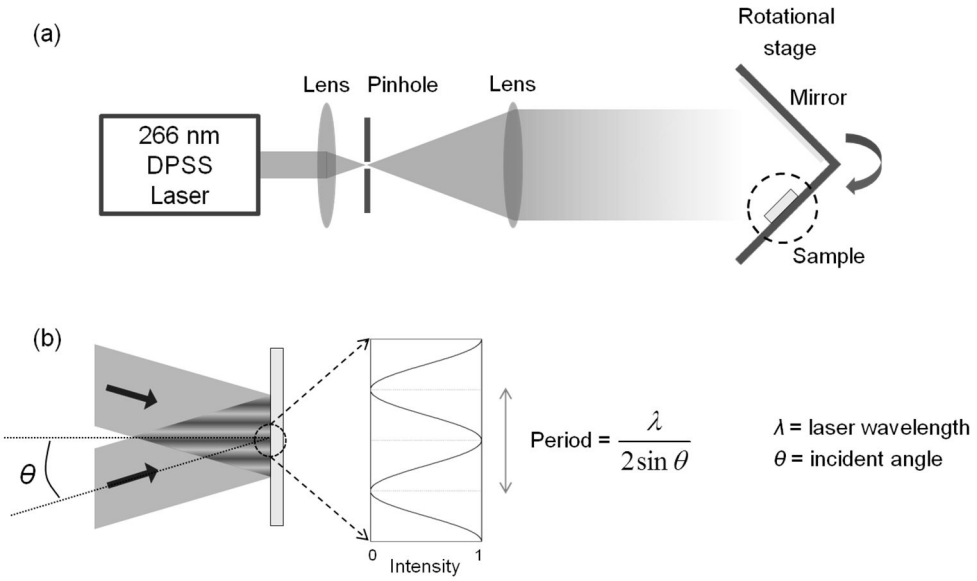

Figure 3-3-1 (a) A schematic diagram of laser holographic lithography setup using 266 nm DPSS laser as a light source. (b) Interference pattern consisting of a periodic series of fringes representing intensity maxima and minima.

3.3.2 Fabrication steps

Fabrication steps of the lateral PC phosphors are shown in Fig. 3-3-2. A silicon nitride layer was deposited by plasma-enhanced chemical vapor deposition (PECVD) on a quartz substrate. The thickness of the silicon nitride layer is 50 nm. After photoresist (PR) spin-coating and baking processes, LHL was applied to generate 1D PC patterns to PR, as shown in Fig. 3-3-3(a). The patterned sample was dry-etched using reactive-ion etching (RIE) method. By N_2 gas addition, etching selectivity of Si_3N_4 over SiO_2 was provided during the RIE process [9]. Acetone was used for cleaning the sample and removing PR residue on the silicon nitride layer. Figure 3-3-3(b) displays a SEM image of the lateral 1D PC backbone for the phosphor structure. And the mixed solution of PVK and QDs was prepared with QD concentration corresponding to 10 mM in molar concentration, which is over limit value of QD concentration in the vertical PC phosphor we discussed in chapter 2. Afterwards, The PVK:QD solution was spin-coated on the sample to construct the lateral PC phosphor. Figure 3-3-3(c) shows a SEM image of a cross section of the QD-coated PC phosphor sample. A phosphor sample for reference was fabricated by QDs spin-coating on the bare quartz substrate.

In the case of fabrication of the lateral 2D PC phosphors, we only need to perform one more LHL step on the 90°-rotated samples [10].

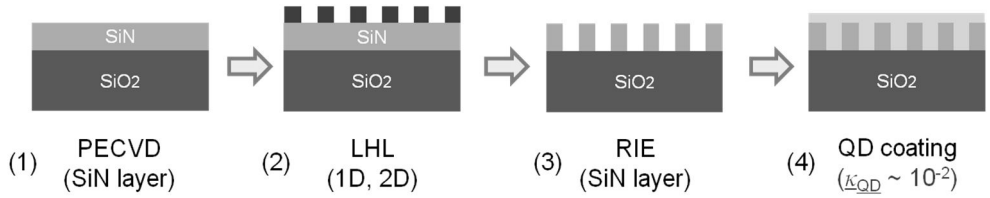

Figure 3-3-2 A Schematic diagram of fabrication steps. (1) A silicon nitride layer was deposited by plasma-enhanced chemical vapor deposition (PECVD) on a quartz substrate. (2) Laser holographic lithography (LHL) was applied to generate 1D PC patterns to PR. (3) The patterned sample was dry-etched using reactive-ion etching (RIE) method. (4) QDs were spin-coated on the sample to construct the lateral PC phosphor.

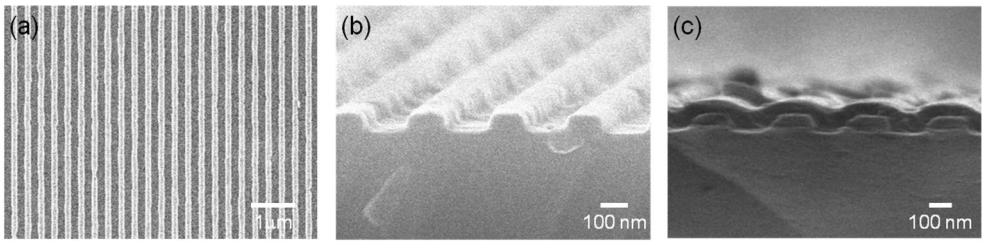

Figure 3-3-3 SEM images of fabricated 1D PCs. (a) Top view of patterned photoresist on the silicon nitride layer. (b) Side view of the dry-etched silicon nitride patterned layer. (c) Side view of the QD-coated PC phosphor sample.

We can notice that there is a broad distinction between the fabricated lateral PC phosphor sample and the ideal lateral PC phosphor modeled in chapter 3.2. Contrary to the ideal PC phosphor which has separate QD regions, the QD layer of the fabricated PC phosphor is continuous and has wavy surface because the QD film was spin-coated. Accordingly, I recalculated the PBE effect and absorption enhancement of the fabricated PC phosphor and compared the fabricated structure and the modeled one. And this time, dispersion relation between the extinction coefficient of the QD and pump wavelength was considered, which was obtained by ellipsometry measurement.

Figure 3-3-4 compares schematics of the fabricated PC phosphor (left) and the modeled PC phosphor (right), which have two points of difference. The fabricated (real) PC phosphor has angled sidewalls while the modeled (ideal) one has vertical sidewalls. And, as mentioned above, the QD layer on the fabricated grating structure has continuous wavy form.

Shown in Fig. 3-3-5 are the calculated absorption spectra of the real PC phosphor, the ideal PC phosphor, and the reference phosphor. Two absorption peaks, which resulted from two PBE modes, were seen clearly in both cases of the real structure and the ideal one. We can now assure that the fabricated wavy structure is a suitable phosphor sample to investigate the PBE effect and expect PL enhancement. Moreover, additional fabrication processes to remove the QD residue on the silicon nitride grating are unnecessary.

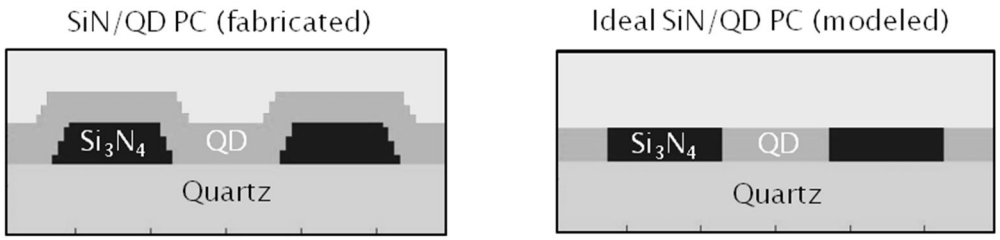

Figure 3-3-4 Schematics of the fabricated PC phosphor (left) and the modeled PC phosphor (right).

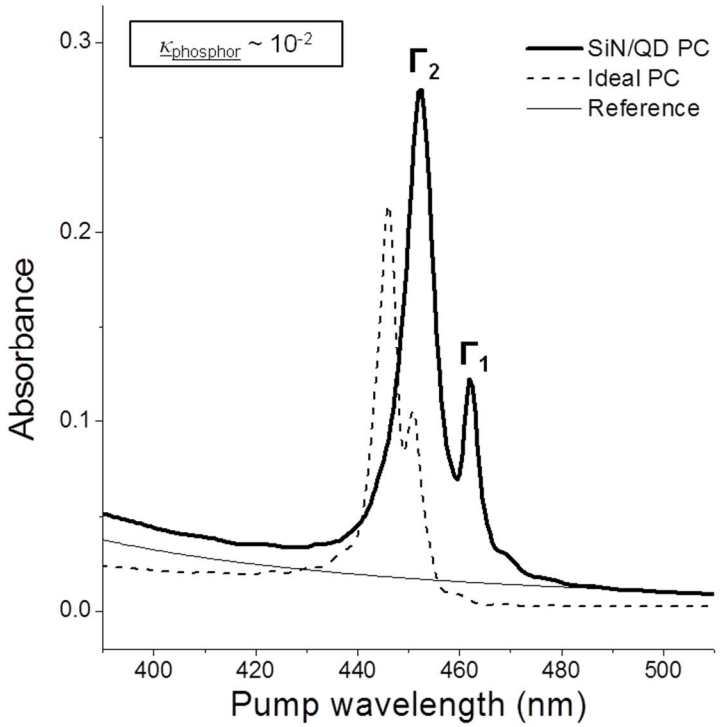

Figure 3-3-5 Calculated absorption spectra of the real PC phosphor, the ideal PC phosphor, and the reference phosphor.

3.4 Measurement and Analyses

3.4.1 Measurement setup

The measurement setup which is introduced in chapter 2 to measure PL as a function of pump wavelength was employed again. Furthermore, I could investigate polarization dependence of the PBE effect by setting a polarizer on the beam pass between the pump source and the phosphor sample.

3.4.2 Photoluminescence enhancement

Figures 3-4-1(a) and 3-4-1(b) show the PL spectra measured for the lateral PC phosphor and the reference phosphor structures, respectively. Like the preceding experiment results about vertical PC phosphors, PL spectra remain unchanged in terms of their peak wavelengths (~580 nm), as well as spectral linewidths (~35 nm in FWHM), regardless of the pump wavelengths. As the pump wavelength changes, however, the peak intensity varies considerably, especially for the PC phosphor.

Figure 3-4-2 displays the measured PL intensity spectra of the lateral PC and the reference phosphor structures, respectively, which intensities are integrated values at each pump wavelengths. There are minor causes of fluctuating PL intensities, e.g. the intensity variation of the pump beam and the extinction coefficient curve of CdSe/ZnS QDs, excluding PBE effects. By obtaining the PL intensity ratio of the lateral PC phosphor to that of the reference phosphor, which is called to the PL enhancement factor, I could consider the PBE effect only.

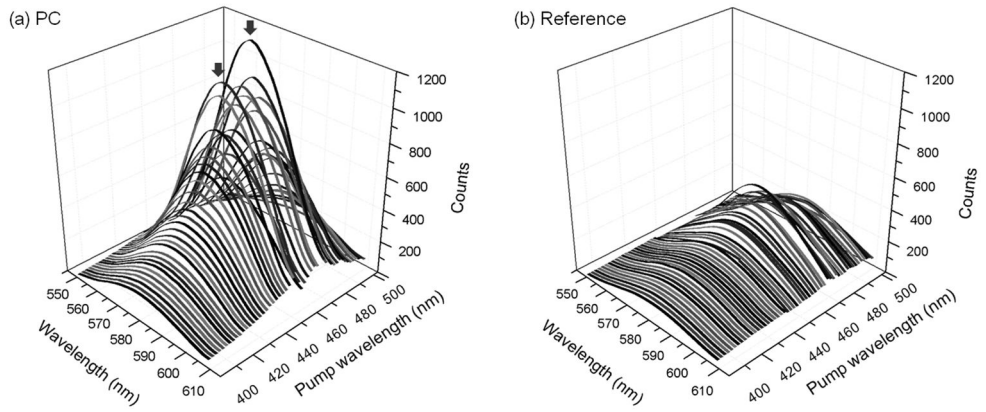

Figure 3-4-1 PL spectra measured as a function of pump wavelength: (a) the lateral PC phosphor and (b) the reference phosphor.

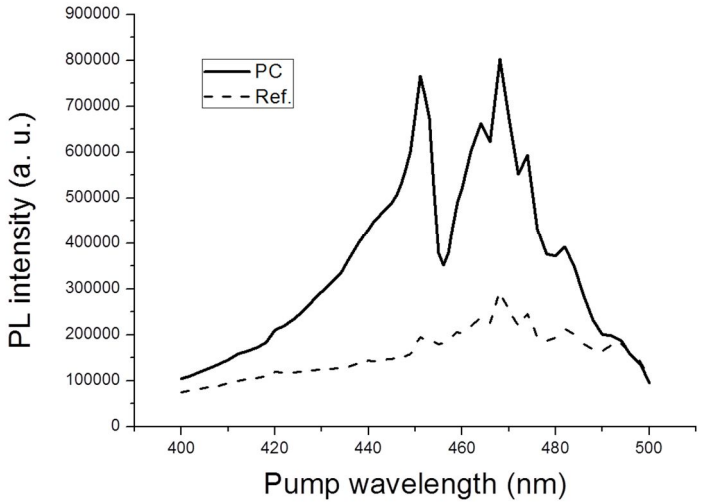

Figure 3-4-2 Measured PL intensity spectra of the lateral PC phosphor (solid line) and the reference phosphor (dashed line) structures.

Shown in Fig. 3-4-3 is the PL enhancement factor at various pump photon wavelengths. We can observe two peaks at correspond Γ–point PBE wavelengths, which as expected by simulations, which results were shown in Fig. 3-3-5. Moreover, Table 3-4-1 compares Γ_1 and Γ_2 PBE wavelengths of measurement data and calculated data. The results of experiments, such as PBE wavelengths and the wavelength spacing between two PBE modes, agree with theoretical assessments.

In spite of high concentration of QDs, the PBE effect in the lateral PC phosphor was observed by experiments and the PL enhancement factor was improved remarkably also, which implies that the lateral PC phosphors have more applicability than the vertical one.

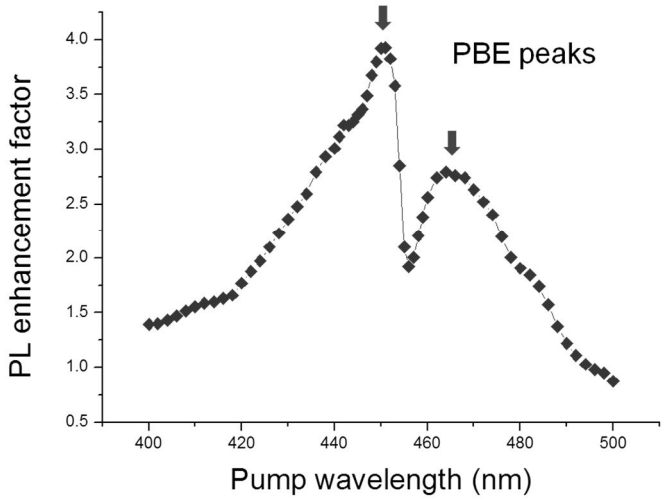

Figure 3-4-3 PL enhancement factor of the lateral 1D PC phosphor.

	Γ_1	Γ_2
Measurement	451 nm	464 nm
Simulation	452 nm	462 nm

Table 3-4-1 Γ_1 and Γ_2 PBE wavelengths of measurement data and calculated data.

3.4.3 Polarization dependence of the photonic band-edge effect

Figure 3-4-4 displays intuitively that the PBE effects in the lateral PC phosphors depend on the polarization of the pump source. In behavior of photons, electric fields are naturally vertical to direction of propagation. The direction of wave vectors of PBE modes of the lateral 1D PC is parallel to periodicity whether $k_{//} = 0$ or not. Either, angle of incidence of external pump photons is perpendicular to the surface. Because direction of wave vectors of PBE modes is certainly normal to propagation of the external pump photons, polarization of the pump source should be defined in only one direction which satisfies all conditions above. In conclusion, the direction of pump polarizaion should be perpendicular to periodicity, which is the direction of *y*-axis explained in Fig 3-2-1(b).

Therefore, we can ensure that the PBE effect affect the PL intensity from the lateral 1D PC phosphor by experiments with polarized pump sources. Figure 3-4-5 shows measured PL intensity spectra of the lateral PC phosphor structures, when polarization angles of the pump source are 0˚ and 90˚, respectively. In case that the angle of pump polarization is zero, which means direction of pump source polarization is normal to periodicity of the lateral 1D PC, PL enhancements at corresponding PBE wavelengths occurred. On the other hand, no specific peaks appeared in the PL intensity spectrum when the pump source is polarized at 90 degree. It is an important proof of the PBE effect in the 1D PC phosphor that peaks in the PL intensity spectrum appeared only when the pump source was polarized suitably.

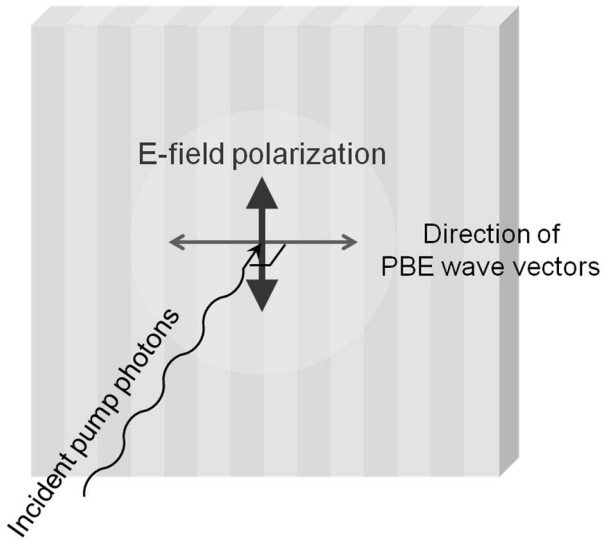

Figure 3-4-4 Polarization dependence of the photonic band-edge effect in the 1D PC.

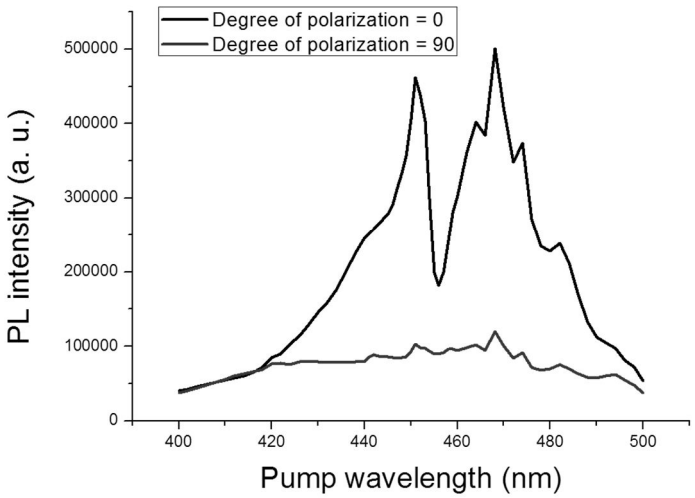

Figure 3-4-5 Measured PL intensity spectra of the lateral 1D PC phosphor structure, when polarization angles of the pump source are 0˚and 90˚, respectively.

On the contrary, PBE effects in the lateral 2D PC phosphors with square lattice patterns having rotational symmetry are independent from the pump source polarization. Figure 3-4-6(a) shows the photonic band structures of the lateral 2D PC phosphor, which was calculated by the PWE method. I called a group of PBE modes of Γ_1, Γ_2, Γ_3, and Γ_4 as Γ_A PBE because and Γ_1, Γ_2, Γ_3, and Γ_4 modes are degenerated and not distinguishable in the photonic band structure and corredsponding absorption spectrum. For the same reason, I called a group of PBE modes of Γ_5, Γ_6, and Γ_7 as Γ_B PBE. We can found absorbance peaks at Γ_A and Γ_B PBE wavelengths in absorbance spectrum shown in Fig. 3-4-6(b) and the electromagnetic fields of the corresspond PBE modes are well-confined at phosphor region, which is described in Fig. 3-4-6(c).

I compared PBE effects and absorbance enhancements of the 2D PC phosphor with pump sources polarized at 0˚,45˚, and 90˚, as can be seen in table 3-4-2. This property about polarization independence of the pump source in the lateral 2D PC phosphor is a great help to apply PC structures to real light-emitting devices.

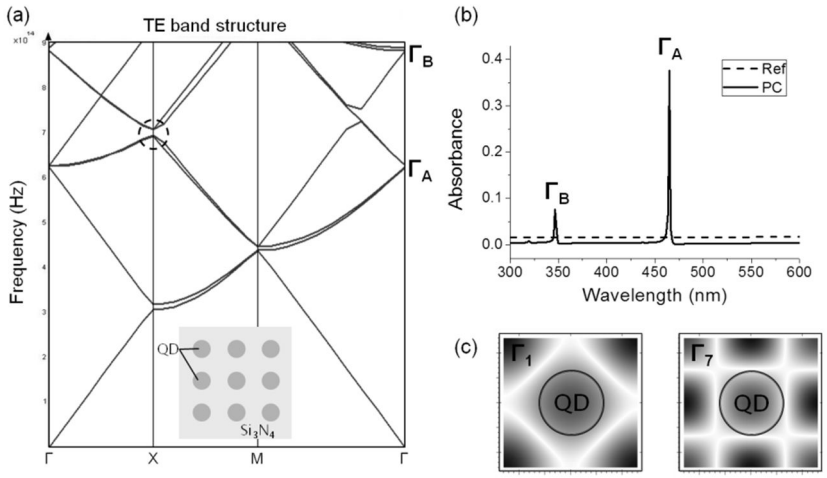

Figure 3-4-6 Properties of a lateral 2D PC phosphor. (a) The photonic band structure and a schematic of the lateral 2D PC phosphor. (b) Absorbance spectra of pump photons in the lateral 2D PC phosphors and the reference phosphors. (c) Magnetic field profiles (H_z) of Γ-point band-edge modes of the 2D PC.

Pol. angle	0°	45°	90°
E-field polarization of a pump source	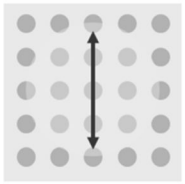	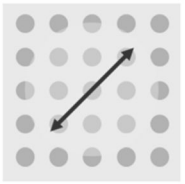	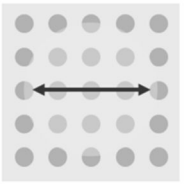
Absorbance spectra	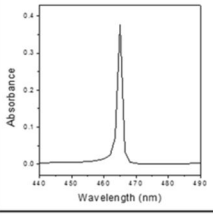	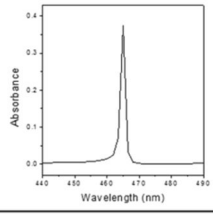	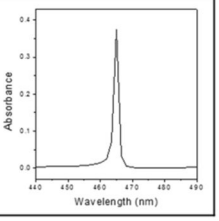

Table 3-4-2 Comparison between absorbance spectra of the lateral 2D PC phosphor with pump sources polarized at 0°, 45°, and 90°.

3.5 Summary

The idea of lateral PC phosphors for improved performance has been developed. Compared to the vertical PC phosphors, the lateral PC phosphors have advantages of applicability in the real optical devices.

Using FDTD simulation tools, the photonic band structures and the properties of the PBE modes of the lateral PCs were explored. The optical fields at PBE wavelengths were spatially confined in the lateral PC phosphor slabs, resulting in improvement of the optical interaction with the phosphor material. And I explained intuitively the reason why the Γ-point PBE mode is suitable for application of the lateral PC phosphors. Pumped by an external source with the Γ-point PBE wavelengths, absorbance of pump photons in the lateral PC phosphor grew stronger than that in the reference phosphor.

I fabricated the corresponding lateral 1D PC phosphor structure, which was patterned using the LH lithography technique. The PVK:QD solution acted as the phosphor material again, and was spin-coated on the patterned substrate. The PL intensities were measured as a function of pump wavelength. As expected, the PL intensity maximized when the pump photon energy was tuned to the Γ-point PBE wavelength. Furthermore, polarization dependence of the photonic band-edge effect in the lateral PC phosphors was assured.

References

[1] K. Min, S. Choi, Y. Choi, and H. Jeon, "Enhanced fluorescence from CdSe/ZnS quantum dot nanophosphors embedded in one-dimensional photonic crystal backbone structure," Nanoscale **6**, 14531-14537 (2014).

[2] S. Kim, Y. Park, K. Hwang, J. Lee, H. Jeon, and H. J. Kim, "High-power and large-alignment-tolerance fiber coupling of honeycomb-lattice photonic crystal Γ-point band-edge laser," J. Opt. Soc. Am. B **26**, 1330-1333 (2009).

[3] J. Mouette, C. Seassal, X. Letartre, P. Rojo-Romeo, J.-L. Leclercq, P. Regreny, P. Viktorovitch, E. Jalaguier, P. Perreau, and H. Moriceau, "Very low threshold vertical emitting laser operation in InP graphite photonic crystal slab on silicon," Electron. Lett. **39**, 526–528 (2003).

[4] M. Imada, S. Noda, A. Chutinan, T. Tokuda, M. Murata, and G. Sasaki, "Coherent two-dimensional lasing action in surface-emitting laser with triangular-lattice photonic crystal structure," Appl. Phys. Lett. **75**, 316–318 (1999).

[5] http://www.lumerical.com

[6] C. Kittel, *Introduction to Solid State Physics, 8th ed.* (Wiley 2004).

[7] J. D. Jackson, *Classical Electrodynamics, 3rd ed.* (Wiley 1998).

[8] D.-Y. Kim, S. K. Tripathy, L. Li, and J. Kumar, "Laser-induced holographic surface relief gratings on nonlinear optical polymer films," Appl. Phys. Lett. **66**, 1166–1168 (1995).

[9] B. E. E. Kastenmeier, P. J. Matsuo, and G. S. Oehrlein, "High selective etching of silicon nitride over silicon and silicon dioxide," J. Vac. Sci. Technol. A **17**,

3179–3184 (1999).

[10] J. H. Moon, S.-M. Yang, D. J. Pine, and W.-S. Chang, “Multiple-exposure holographic lithography with phase shift,” Appl. Phys. Lett. **85**, 4184–4186 (2004).

Chapter 4

Conclusion

I have proposed two kinds of PCs as novel phosphor structures for enhanced luminous efficiency. When photons of a PBE mode are incident onto the PC structures, the optical field builds up intensively inside the structure, offering an opportunity to largely strengthen the optical interaction with the materials. Consequently, if an optically active phosphor agent is introduced into such a structure, the absorption of incident photons can be maximized when the photon energy is tuned to a PBE.

At first, following the initial theoretical estimation, I fabricated the vertical PC phosphor structure by alternately spin-coating two kinds of polymer materials, PVK:QD and CA, up to 15 layer pairs. CdSe/ZnS core-shell QDs were dispersed in PVK, so that only the high refractive index layers could fluoresce. As anticipated from the theoretical calculations, the photoluminescence intensity became highest when the pump photon energy coincided with the first reflectance minimum, which is a PBE of the corresponding vertical PC with a finite number of layer pairs. In comparison with a reference phosphor that corresponds to a bulk phosphor, the PL intensity from the PC phosphor was improved by a factor of 1.36.

In order to improve performance of the PC phosphors, I realized the lateral PC phosphor. Theoretical simulations showed that PL enhancement occurs when the pump photon energy is tuned to a band-edge where $k_{//} = 0$, which is the Γ–point PBE of the lateral PC. A silicon nitride grating on a quartz substrate was fabricated with laser holographic lithography and high concentration QDs are coated on the

grating. I investigated the PL enhancement by the Γ–point PBE effect as well as polarization dependence of a pump source on the PL enhancement.

I believe that this approach to improve the PL efficiency by nano-structuring a phosphor material is a paradigm shift from the conventional approach of developing new phosphor materials. Our PC phosphor scheme is not bound to a specific phosphor, but can be generally applied to any material. Further structural optimization of the PC phosphor, when combined with a future phosphor material with an extremely high efficiency, could have a significant impact on phosphors and other related applications, such as white LEDs, for which the improvement of the PL efficiency is a key area of development.

국문 초록

광자결정은 굴절률이 서로 다른 두 가지 이상의 물질이 공간 상에서 주기적으로 배열되어 있는 광학 구조를 말한다. 고체 결정에서 주기적인 포텐셜의 존재로 인해 전자의 에너지 밴드 및 밴드갭이 형성되는 것과 유사한 원리로, 광자결정의 주기성에 의해 광밴드구조에서 광밴드갭 주파수 영역이 나타나며, 광밴드갭 대역에 해당하는 빛은 광자결정 내부를 진행할 수 없다. 한편, 광밴드갭 대역의 경계에 해당하는 광밴드에지 주파수에서는 독특하고 흥미로운 특징을 가진 전자기장 모드가 나타난다. 광밴드에지 파장에 해당하는 빛의 군속도는 0에 가까운 값을 가지며, 그 결과 빛과 물질의 상호 작용이 크게 증가한다.

형광체 물질에서는 빛의 파장 변환 현상이 진행된다. 즉, 형광체는 여기 광자의 에너지를 흡수하여 여기 광자와 다른 파장의 광자를 방출하며, 일반적인 경우 방출 광자의 파장은 여기 광자의 파장보다 길다. 이러한 형광체의 색 변환 특성은 일반 조명 산업에서 널리 응용되고 있다. LED나 레이저와 같은 여기 광원에 형광체가 결합된 형태로 백색의 빛을 발하는 발광소자는 현재 가장 진보된 조명 광원으로서 관심을 받고 있고, 그에 따라 형광체의 발광 효율을 증가시키기 위한 다양한 연구가 진행되었다. 그러나 대부분의 업적은 새로운 화학 물질의 합성이나 도입을 통해 형광체의 내부 양자 효율을 증가시키는 방법으로, 형광체 자체의 물성에 주목하고 있다.

본 학위 논문에서는, 형광체 물질의 광펌핑 효율을 증가시키기 위한 방법으로 광자결정 형광체라는 새로운 개념을 제시한다. 형광체의 내부 양자 효율이나 광추출 효율을 개선시키기 위한 기존의 다른 방법과는 달리 구조적인 측면에서 접근하여, 구조화된 형광체 영역에 여기 광자의 집중도를 높이고자

하였다. 구체적으로 광자결정 형광체의 광밴드에지 모드의 전기장은 구조 내부에 국지화되므로, 여기 광자와 형광체 물질 사이의 상호 작용이 크게 증가할 것이다. 본 논문에서는 광자결정의 주기 방향에 따라 수직 방향과 측 방향, 두 가지 종류의 광자결정 형광체를 제시하였다.

핵심어: 광자결정, 형광체, 광자결정 형광체, 광밴드에지, 양자점, 레이저 홀로그래픽 리쏘그래피

학번: 2007-22865